

# General Perturbative Approach for Spectroscopy, Thermodynamics, and Kinetics: Methodological Background and Benchmark Studies

Julien Bloino,<sup>\*,†,§</sup> Malgorzata Biczysko,<sup>‡</sup> and Vincenzo Barone<sup>\*,†</sup>

<sup>†</sup>Scuola Normale Superiore, piazza dei Cavalieri 7, I-56126 Pisa, Italy

<sup>‡</sup>Center for Nanotechnology Innovation @NEST, Istituto Italiano di Tecnologia, Piazza San Silvestro 12, I-56127 Pisa, Italy

<sup>§</sup>Consiglio Nazionale delle Ricerche, Istituto di Chimica dei Composti Organometallici (CNR-ICCOM), UOS di Pisa, Via G. Moruzzi, 1 I-56124 Italy

**ABSTRACT:** A general second-order perturbative approach based on resonance- and threshold-free computations of vibrational properties is introduced and validated. It starts from the evaluation of accurate anharmonic zero-point vibrational energies for semirigid molecular systems, in a way that avoids any singularity. Next, the degeneracy corrected second-order perturbation theory (DCPT2) is extended to a hybrid version (HDCPT2), allowing for reliable computations even in cases where the original formulation faces against severe problems, including also an automatic treatment of internal rotations through the hindered-rotor model. These approaches, in conjunction with the so-called simple perturbation theory (SPT) reformulated to treat consistently both energy minima and transition states, allow one to evaluate degeneracy-corrected partition functions further used to obtain vibrational contributions to properties like enthalpy, entropy, or specific heat. The spectroscopic accuracy of the HDCPT2 model has been also validated by computing anharmonic vibrational frequencies for a number of small-to-medium size, closed- and open-shell, molecular systems, within an accuracy close to that of well established but threshold-dependent perturbative-variational models. The reliability of the B3LYP/aug-N07D model for anharmonic computations is also highlighted, with possible improvements provided by the B2PLYP/aug-cc-pVTZ models or by hybrid schemes. On a general grounds, the overall approach proposed in the present work is able to provide the proper accuracy to support experimental investigations even for large molecular systems of biotechnological interest in a fully automated manner, without any *ad hoc* scaling procedure. This means a fully *ab initio* evaluation of thermodynamic and spectroscopic properties with an overall accuracy of about, or better than, 1 kJ mol<sup>-1</sup>, 1 J mol<sup>-1</sup> K<sup>-1</sup> and 10 cm<sup>-1</sup> for enthalpies, entropies, and vibrational frequencies, respectively.

## 1. INTRODUCTION

Theoretical models to account for molecular vibrations are among the most important tasks of contemporary computational chemistry.<sup>1–3</sup> In fact, vibrational frequencies and vibrational partition functions ( $Q_{\text{vib}}$ ) play a central role in a number of physical–chemical processes spanning from structural characterization of molecular systems, whose experimental spectra are seldom straightforward to interpret,<sup>4</sup> to thermodynamic equilibria and kinetic parameters.<sup>5</sup> The harmonic oscillator model has been for a long time the reference level for such quantities, and the availability of computers of increasing power coupled to the development of accurate and effective quantum mechanical (QM) approaches has led to a very fruitful synergy between experimental results and computations for molecular systems of increasing size. Improved accuracy has been obtained by suitable scaling factors accounting for both limitations of the QM treatment and neglect of anharmonicity.<sup>6</sup> However, different scaling factors must be used for vibrational frequencies, zero-point energies ( $E_0$ ), and partition functions due to the different role of anharmonicity in these diverse quantities. For this reason, the definition of consistent procedures making use of various scaling factors depending on the vibrational properties is rather cumbersome. This matter has been recently discussed with particular emphasis on their uncertainties, accuracy, and consistency.<sup>7–9</sup> It should be noted that the most advanced composite thermochemical procedures developed until now to compute accurate energies<sup>10–15</sup> can reach for small molecules an average error as low as 0.2 kJ mol<sup>-1</sup> with respect to highly accurate

experimental atomization energies.<sup>10</sup> However, if larger systems are to be considered, such schemes still resort to the scaling of harmonic frequencies,<sup>16–18</sup> leading to an overall accuracy of ~4 kJ mol<sup>-1</sup> (1 kcal mol<sup>-1</sup>). In fact, it has been pointed out that, at least for species containing many hydrogens, the factor limiting accuracy of thermochemical protocols will increasingly be the quality of the zero-point vibrational energy.<sup>19</sup>

Recently, development and validation of true anharmonic approaches even for quite large systems are paving the route toward reliable computations of all the diverse quantities mentioned above without the need of any *ad hoc* scaling factor. Two main routes to develop and implement vibrational computations beyond the harmonic approximation went through perturbative<sup>20–32</sup> and variational approaches.<sup>3,33–41</sup> In particular, the second-order perturbative vibrational treatment<sup>20–24,32</sup> (hereafter referred to as VPT2) provides remarkably accurate results for both fundamental frequencies and  $E_0$ , at least for semirigid systems. An efficient approach is obtained when VPT2 is applied to a fourth-order representation of the potential energy surface (PES) evaluated by means of Density Functional Theory (DFT) using hybrid (especially B3LYP<sup>42–48</sup>) or double-hybrid (especially B2PLYP<sup>49–51</sup>) functionals in conjunction with medium-size basis sets. Further improvements in accuracy can be obtained by computing the harmonic part of the force field at a more refined

Received: November 13, 2011

Published: February 2, 2012

level, with the coupled cluster (CC) method providing the most effective route, at least in the absence of strong multireference character.<sup>42,48,52–55</sup>

On the grounds of the accuracy and feasibility of VPT2 computations, Truhlar and Isaacson proposed a method, called simple perturbation theory (SPT),<sup>56</sup> to approximate  $Q_{\text{vib}}$ , which provided remarkable results compared to accurate computations.<sup>56–61</sup> In this model,  $Q_{\text{vib}}$  at temperature  $T$  is given by

$$Q_{\text{vib}} = \frac{e^{-hcE_0/k_B T}}{\prod_i (1 - e^{-hc\nu_i/k_B T})}$$

where the zero of energy is at the bottom of the vibrational well, and where the zero point energy  $E_0$  and the fundamental excitation energies  $\nu_i$  are evaluated at the VPT2 level.

However, it is well-known that perturbation theory has singularities when one frequency is close to twice another one or to the sum of two others, these situations being generally known as resonance. It is standard practice, leading to the generalized second-order vibrational perturbation (GVPT2) approach, to remove these resonances from the perturbative treatment (deperturbed approach, DVPT2) and to treat them in a second step by proper reduced dimensionality variational computations.<sup>20,21,23,25</sup> This is a sound procedure for individual cases, but due to the arbitrary definition of resonant terms it faces severe difficulties whenever one has to consider a series of force fields for a given system, or a series of geometries along a reaction path. As a matter of fact, the switching on and off of specific resonances is not smooth and introduces annoying discontinuities in the computations. A viable solution to this problem is offered by the so-called degeneracy-corrected second-order perturbation theory (DCPT2), first introduced by Truhlar and co-workers<sup>60</sup> and since then rediscovered by other authors.<sup>62,63</sup> DCPT2 corresponds to a resummation of higher-order terms, providing the infinite-order result for a resonance and reducing to VPT2 results far from resonances. While several studies, including comparisons with accurate variational results for model systems, suggested that DCPT2 can become a method of choice for a black-box implementation of anharmonic computations of medium-to-large semirigid systems,<sup>60,61,63</sup> it suffers severe problems when very strong couplings between low- and high-frequency vibrations occur. To overcome this shortcoming, we propose here a hybrid degeneracy-corrected VPT2 (HDCPT2) model based on switching off and on between DCPT2 and VPT2 approaches in a way to avoid problems related to degeneracies and near-degeneracies as well as those with the validity of assumptions used to derive DCPT2 terms, leading finally to a truly general and black-box procedure to compute anharmonic frequencies.

The situation is more involved for partition functions since the use of DCPT2 affects the predicted value of  $E_0$ , which can have, in turn, a major effect on  $Q_{\text{vib}}$  at low temperatures. A possible solution to this problem is to consider all cubic interactions to be resonant, leading to the so-called resonance-corrected second-order perturbation theory (RCPT2).<sup>61</sup> One important feature of this method is that whether cubic interactions are treated as resonant or not does not affect  $E_0$ , which represents the largest contribution to  $Q_{\text{vib}}$  at low temperatures. Since, however, vibrational frequencies depart from their most accurate values, we are falling again into the unsatisfactory situation of using different models for spectroscopy and kinetics/thermodynamics.

Fortunately, it has been recently shown that for asymmetric tops, it is possible to recast the anharmonic contribution to  $E_0$  in a

way that avoids any singularity.<sup>64</sup> With a view to obtain also accurate kinetic parameters, we extend here this resonance-free approach to transition states. Use of this formulation together with the HDCPT2 model paves the route toward a fully coherent black box evaluation of spectroscopic, thermodynamic, and kinetic effects (see Figure 1) by second-order perturbation theory.

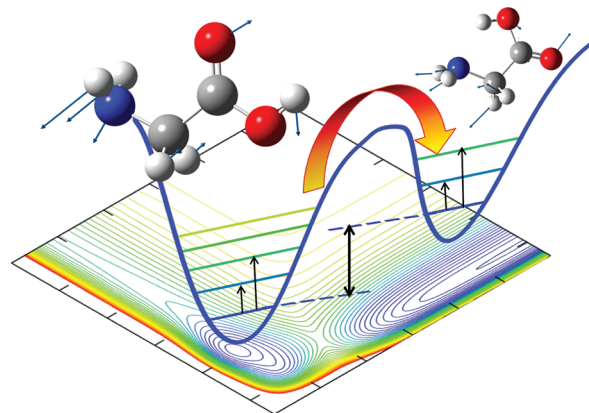


**Figure 1.** General model to include anharmonic vibrational effects: spectroscopy, thermodynamics, and kinetics.

The present work is thus devoted to the implementation and validation of this approach for a number of molecular systems. The current finite difference evaluation of cubic and quartic force constants can be used with any QM model for which analytical Hessians are available. This means that, together with isolated molecules, we can treat also systems in solution using the polarizable continuum model (PCM).<sup>65–68</sup>

The paper is organized as follows. In section 2, the HDCPT2 model is introduced, providing also a detailed analysis of the underlying theoretical framework. Then, details about QM computations are gathered in section 3. Finally, extensive benchmark results on the zero-point vibrational energies (ZPVE), partition functions, entropies, and vibrational frequencies are reported and discussed in sections 4.1–4.3. The paper ends with conclusions about the applicability of the presented approach, emphasizing its black-box assets.

## 2. THEORY

The method presented below is intended to be general enough to treat both energy minima and transition states, provided that, in the latter case, the reaction coordinate is assumed uncoupled from the rest of the vibrational modes. The  $N$  normal modes of the system can be subdivided into  $N_R$  elements associated with real frequencies ( $N_R \geq N - 1$ ) and  $N_I$  modes with imaginary frequencies along the reaction coordinates, so that,

$$N = N_R + N_I$$

For a molecule about an equilibrium geometry,  $N_R = N$  and  $N_I = 0$ , while at a transition state,  $N_I = 1$  and  $N_R = N - 1$ . In the following, we will use the subscript  $F$  to designate the mode with an imaginary frequency

The harmonic vibration partition function,  $Q_{\text{vib}}^H(T)$  is given by

$$Q_{\text{vib}}^H(T) = \frac{e^{-hcE_0^{(0)}/k_B T}}{\prod_{i=1}^{N_R} (1 - e^{-\varepsilon_i/k_B T})} \quad (1)$$

where  $T$  is the temperature and  $k_B$  the Boltzmann constant.  $E_0^{(0)}$  is the harmonic ZPVE (in  $\text{cm}^{-1}$ ), obtained by summing the real vibrational frequencies, and  $\varepsilon_i = hc\omega_i$ ,  $\omega_i$  being the harmonic frequency of mode  $i$ , expressed in wavenumbers.

As mentioned in the Introduction, the simple perturbation theory proposed by Truhlar and Isaacson<sup>56</sup> offers a simplified and straightforward application of perturbation theory to the harmonic vibrational partition function, by replacing  $E_0^{(0)}$  and  $\omega_i$  with their anharmonic counterparts, respectively  $E_0$  and the fundamental energies  $\nu_i$ , calculated with second-order perturbation theory. The vibrational partition function  $Q_{\text{vib}}(T)$  obtained this way is

$$Q_{\text{vib}} = \frac{e^{-hcE_0/k_B T}}{\prod_{i=1}^{N_R} (1 - e^{-hc\nu_i/k_B T})} \quad (2)$$

in which all normal modes, including the reaction coordinate  $F$ , are assumed to be formally uncoupled.

Let us first define the anharmonic ZPVE for asymmetric tops, starting from the expression of a molecular vibrational energy (expressed in  $\text{cm}^{-1}$ ):

$$E(n) = \chi_0 + \sum_{i=1}^N \omega_i \left( n_i + \frac{1}{2} \right) + \sum_{i=1}^N \sum_{j=i}^N \chi_{ij} \left( n_i + \frac{1}{2} \right) \left( n_j + \frac{1}{2} \right) \quad (3)$$

where  $\chi_0$  and  $\chi_{ij}$  have been defined previously<sup>23</sup> and  $n_i$  represents the quantum number associated to mode  $i$ . Note also that, as already pointed out,<sup>23</sup> symmetric tops can be treated as well, with negligible numerical errors, provided that the mass of one atom is slightly changed (on the order of  $10^{-3}$  amu) in order to reduce the symmetry to that of an Abelian group.

For a system in an energy minimum, an expression of the anharmonic ZPVE devoid of singularities has been proposed by Schuurman et al.,<sup>64</sup> starting from

$$E_0 = \chi_0 + \sum_{i=1}^N \frac{\omega_i}{2} + \sum_{i=1}^N \sum_{j=i}^N \frac{\chi_{ij}}{4}$$

In order to extend it to transition states, we divide the vibrational energy into two terms, one for the reaction coordinate with an imaginary frequency and the other containing the remaining  $N_R$  modes. For the latter term, the definition of the contribution to ZPVE is unambiguous and equal to the previous expression, using  $N$  elements for the summations. However, the contribution of the reaction coordinate to the ZPVE is more equivocal. Considering the possible application to the calculation of reaction rate constants, it has been chosen to include only the real contribution related to the reaction coordinate  $F$  in the  $\chi_0$  term, noted  $\chi_0^F$  in the following. Hence, we define  $E_0$  with the relation

$$E_0 - E_0^{(0)} = a \sum_{i=1}^{N_R} \sum_{j=1}^{N_R} \left\{ \frac{K_{ijij}}{32\hbar \sqrt{\lambda_i \lambda_j}} - \sum_{k=1}^{N_R} \frac{1}{\sqrt{\lambda_i \lambda_j \lambda_k}} \times \left[ \frac{K_{iik} K_{jjk}}{32\omega_k} + \frac{K_{ijk}^2}{48(\omega_i + \omega_j + \omega_k)} \right] \right\} + Z_{\text{kinetic}} + \chi_0^F \quad (4)$$

with  $\lambda_i^{1/2} = 2\pi c\omega_i$  and  $a = \hbar^3$ .  $K_{ijk}$  and  $K_{ijkl}$  are respectively the third and fourth derivatives of the potential energy (expressed here in wavenumbers) with respect to the mass-weighted normal coordinates  $Q$ :

$$K_{ijk} = \frac{\partial^3 V}{\partial Q_i \partial Q_j \partial Q_k}, \quad K_{ijkl} = \frac{\partial^4 V}{\partial Q_i \partial Q_j \partial Q_k \partial Q_l}$$

and  $Z_{\text{kinetic}}$  is the kinetic contribution to the energy:<sup>23</sup>

$$Z_{\text{kinetic}} = 16 \sum_{\tau=x,y,z} \mu_{\tau\tau}^{\text{eq}} \left[ 1 + \sum_{i=1}^{N_R-1} \sum_{j=i+1}^{N_R} (\zeta_{ij}^{\tau})^2 \right] \quad (5)$$

$\mu_{\tau\tau}^{\text{eq}}$  is an element of the inverse inertia tensor at the reference geometry;  $\zeta_{ij}^{\tau}$  is a Coriolis coupling.

$\chi_0^F$  represents the contribution related to the imaginary frequency  $F$ :

$$\frac{64\chi_0^F}{a} = \frac{K_{FFFF}}{\hbar\lambda_F} - \frac{7K_{FFF}^2}{9\lambda_F^2} + \sum_{j=1}^N \left\{ \frac{3K_{jFF}^2}{\lambda_F(4\lambda_F - \lambda_j)} + \frac{3K_{Fjj}^2}{\lambda_j(4\lambda_j - \lambda_F)} \right\} - \sum_{j=1}^N \sum_{k=1}^{j-1} \frac{16K_{Fjk}^2}{\Delta_{Fjk}} \quad (6)$$

with

$$\Delta_{Fjk} = \lambda_F^2 + \lambda_j^2 + \lambda_k^2 - 2(\lambda_F\lambda_j + \lambda_F\lambda_k + \lambda_j\lambda_k)$$

Real fundamental excitation bands at the VPT2 level are given by

$$\nu_i - \omega_i = 2S_{ii} + 2N_{ii} + 2T_{ii} + \frac{1}{2} \sum_{i=1}^N \sum_{j \neq i} [S_{ij} + N_{ij} + T_{ij}] \quad (7)$$

where  $N$  and  $S$  correspond to the real nonresonant and potentially resonant terms, respectively. The meaning of these terms will be clarified later.  $T$  refers to the terms with imaginary frequencies (transition vector), when present. From now on, we consider the more general case of a transition state, with an imaginary frequency  $\omega_F$ , so that all six terms of eq 7 are included. They are given by the relations

$$A_{ii}N_{ii} = \frac{K_{iiii}}{\hbar} - \frac{5K_{iii}^2}{3\lambda_i} \quad (8)$$

$$A_{ii}S_{ii} = - \sum_{j=1}^{N_R} \frac{(8\lambda_i - 3\lambda_j)K_{ijj}^2}{\lambda_j(4\lambda_i - \lambda_j)} \quad (9)$$

$$A_{ii}T_{ii} = - \frac{(8\lambda_i - 3\lambda_F)K_{iif}^2}{\lambda_F(4\lambda_i - \lambda_F)} \quad (10)$$

$$B_{ij}\mathcal{N}_{ij} = \frac{K_{ijj}}{\hbar} - \frac{K_{iij}K_{ijj}}{\lambda_i} - \frac{K_{jjj}K_{ijj}}{\lambda_j} - \sum_{k=1}^{N_R} \frac{K_{iik}K_{jjk}}{\lambda_k} + \frac{4(\lambda_i + \lambda_j)}{a} \sum_{\tau=x,y,z} \mu_{\tau\tau}^{\text{eq}}(\zeta_{ij}^{\tau})^2 \quad (11)$$

$$B_{ij}\mathcal{S}_{ij} = -\frac{2K_{ijj}^2}{4\lambda_i - \lambda_j} - \frac{2K_{ijj}^2}{4\lambda_j - \lambda_i} + \sum_{k=1}^{N_R} \frac{2(\lambda_i + \lambda_j - \lambda_k)K_{ijk}^2}{\Delta_{ijk}} \quad (12)$$

$$B_{ij}\mathcal{T}_{ij} = \frac{2(\lambda_i + \lambda_j - \lambda_F)K_{ijF}^2}{\Delta_{ijF}} - \frac{K_{iif}K_{jff}}{\lambda_F} \quad (13)$$

with

$$A_{ii} = \frac{16}{a}\lambda_i$$

$$B_{ij} = \frac{4}{a}\sqrt{\lambda_i\lambda_j}$$

$$\Delta_{ijk} = \lambda_i^2 + \lambda_j^2 + \lambda_k^2 - 2(\lambda_i\lambda_j + \lambda_i\lambda_k + \lambda_j\lambda_k)$$

For  $\Delta_{ijF}$ , we use the expression given in ref 69:

$$\Delta_{ijF} = (2\pi c)^4 [(\omega_i + \omega_j)^2 - \omega_F^2][(\omega_i - \omega_j)^2 - \omega_F^2] \quad (14)$$

$\omega_F$ , the imaginary frequency, can be rewritten:

$$\omega_F = i\mathcal{I}(\omega_F)$$

with  $\mathcal{I}(\omega_F)$  real. By replacing  $\omega_F$  with the previous relation,  $\Delta_{ijF}$  is given by

$$\Delta_{ijF} = (2\pi c)^4 [(\omega_i + \omega_j)^2 + \{\mathcal{I}(\omega_F)\}^2] \times [(\omega_i - \omega_j)^2 + \{\mathcal{I}(\omega_F)\}^2] \quad (15)$$

With the same transformation,  $\mathcal{T}_{ii}$  becomes

$$\mathcal{T}_{ii} = +\frac{a}{16(2\pi c)^4} \frac{(8\omega_i^2 + 3\{\mathcal{I}(\omega_F)\}^2)K_{iif}^2}{\omega_i^2\{\mathcal{I}(\omega_F)\}^2(4\omega_i^2 + \{\mathcal{I}(\omega_F)\}^2)} \quad (16)$$

A major issue of treating molecular vibrations with perturbation theory is the possible presence of singularities in several terms, which strongly spoils the accuracy of VPT2 calculations. Since modes  $i$  and  $j$  have real frequencies in eq 7, then only  $\mathcal{S}_{ii}$  and  $\mathcal{S}_{ij}$  can be resonant. Singularities in  $\mathcal{S}_{ii}$  and  $\mathcal{I}_{ij}$  occur when resonances,  $\omega_i \approx 2\omega_j$  or  $\omega_i \approx \omega_j + \omega_k$ , are present.<sup>70,71</sup> The most common treatment is to use a threshold to identify the cases of resonances and near-resonances. The resonant terms are then discarded from the perturbative treatment and considered consecutively with a reduced-dimensionality variational approach.<sup>23</sup>

An alternative method, proposed by Kuhler et al.,<sup>60</sup> is to replace *a priori* the possibly resonant terms, as follows. First,

$\mathcal{S}_{ii}$  and  $\mathcal{S}_{ij}$  are developed by means of the partial fraction decomposition:

$$\mathcal{S}_{ii} = -\frac{a}{16(2\pi c)^4\omega_i^2} \sum_{j=1}^N \left[ \frac{2K_{ijj}^2}{\omega_j^2} + \frac{K_{ijj}^2}{2\omega_j(2\omega_i + \omega_j)} - \frac{K_{ijj}^2}{2\omega_j(2\omega_i - \omega_j)} \right]_{j \neq i} \quad (17)$$

$$\mathcal{S}_{ij} = \frac{a}{4(2\pi c)^4\omega_i\omega_j} \left\{ -\frac{K_{ijj}^2}{\omega_j(2\omega_i + \omega_j)} + \frac{K_{ijj}^2}{\omega_j(2\omega_i - \omega_j)} - \frac{K_{ijj}^2}{\omega_i(2\omega_j + \omega_i)} + \frac{K_{ijj}^2}{\omega_i(2\omega_j - \omega_i)} - \sum_{k=1}^{N_R} \left[ \frac{K_{ijk}^2}{2\omega_k(\omega_i + \omega_j + \omega_k)} + \frac{K_{ijk}^2}{2\omega_k(\omega_k - \omega_i - \omega_j)} - \frac{K_{ijk}^2}{2\omega_k(\omega_i - \omega_j - \omega_k)} \right] \right\} \quad (18)$$

Using an analogy with the simplified Hamiltonian,

$$\hat{H} = \begin{pmatrix} A - \varepsilon & k \\ k & A + \varepsilon \end{pmatrix}$$

whose eigenvalues are  $E = A \pm \varepsilon(1 + k^2/\varepsilon^2)^{1/2}$ , they showed that it is possible to rewrite the potentially resonant terms using the transformation:

$$\frac{Sk^2}{2\varepsilon} \rightarrow S(\sqrt{\varepsilon^2 + k^2} - \varepsilon) \quad (19)$$

where  $\varepsilon$  corresponds to half the absolute value of the frequency difference, which may cause the singularity,  $k^2$  is the absolute value of the constant term, and  $S$  is the sign, either equal to +1 or -1.

As an example, let us write the equivalency table for the resonant term in  $\mathcal{S}_{ii}$ ,

$$\frac{a}{32(2\pi c)^4\omega_i^2\omega_j} \frac{K_{ijj}^2}{(2\omega_i - \omega_j)} \rightarrow \begin{cases} k^2 = \frac{aK_{ijj}^2}{32(2\pi c)^4\omega_i^2\omega_j} \\ \varepsilon = \frac{|2\omega_i - \omega_j|}{2} \\ S = \text{sign}\{2\omega_i - \omega_j\} \end{cases} \quad (20)$$

By applying the transformation given in eq 19, we obtain,

$$\frac{a}{32(2\pi c)^4\omega_i^2\omega_j} \frac{K_{ijj}^2}{(2\omega_i - \omega_j)} \rightarrow \text{sign}\{2\omega_i - \omega_j\} \left[ \sqrt{\frac{aK_{ijj}^2}{32(2\pi c)^4\omega_i^2\omega_j} + \left| \frac{2\omega_i - \omega_j}{2} \right|^2} - \left| \frac{2\omega_i - \omega_j}{2} \right| \right] \quad (21)$$



By doing the same for each term in  $\mathcal{S}_{ij}$ , we obtain the following expressions for  $\mathcal{S}_{ii}$  and  $\mathcal{S}_{ij}$ :

$$\begin{aligned} \tilde{\mathcal{S}}_{ii} = & -\frac{a}{16(2\pi c)^4 \omega_i^2} \sum_{j=1}^N \left[ \frac{2K_{ij}^2}{\omega_j^2} + \frac{K_{ij}^2}{2\omega_j(2\omega_i + \omega_j)} \right] \\ & + \sum_{j=1}^N \text{sign}\{2\omega_i - \omega_j\} \\ & \times \left[ \sqrt{\frac{aK_{ij}^2}{32(2\pi c)^4 \omega_i^2 \omega_j} + \left| \frac{2\omega_i - \omega_j}{2} \right|^2} \right. \\ & \left. - \left| \frac{2\omega_i - \omega_j}{2} \right| \right] \end{aligned} \quad (22)$$

$$\begin{aligned} \tilde{\mathcal{S}}_{ij} = & \frac{a}{4(2\pi c)^4 \omega_i \omega_j} \left\{ -\frac{K_{ij}^2}{\omega_j(2\omega_i + \omega_j)} - \frac{K_{ij}^2}{\omega_i(2\omega_j + \omega_i)} \right\} \\ & + \text{sign}\{2\omega_i - \omega_j\} \left[ \sqrt{\frac{aK_{ij}^2}{4(2\pi c)^4 \omega_i \omega_j^2} + \left| \frac{2\omega_i - \omega_j}{2} \right|^2} \right. \\ & \left. - \left| \frac{2\omega_i - \omega_j}{2} \right| \right] + \text{sign}\{2\omega_j - \omega_i\} \\ & \times \left[ \sqrt{\frac{aK_{ij}^2}{4(2\pi c)^4 \omega_i^2 \omega_j} + \left| \frac{2\omega_j - \omega_i}{2} \right|^2} - \left| \frac{2\omega_j - \omega_i}{2} \right| \right] \\ & - \sum_{k=1}^N \left\{ \frac{aK_{ijk}^2}{8(2\pi c)^4 \omega_i \omega_j \omega_k (\omega_i + \omega_j + \omega_k)} \right. \\ & + \text{sign}\{w_k - w_i - w_j\} \\ & \times \left[ \sqrt{\frac{aK_{ijk}^2}{8(2\pi c)^4 \omega_i \omega_j \omega_k} + \left| \frac{\omega_k - \omega_i - \omega_j}{2} \right|^2} \right. \\ & \left. - \left| \frac{\omega_k - \omega_i - \omega_j}{2} \right| \right] - \text{sign}\{\omega_i - \omega_j - \omega_k\} \\ & \times \left[ \sqrt{\frac{aK_{ijk}^2}{8(2\pi c)^4 \omega_i \omega_j \omega_k} + \left| \frac{\omega_i - \omega_j - \omega_k}{2} \right|^2} \right. \\ & \left. - \left| \frac{\omega_i - \omega_j - \omega_k}{2} \right| \right] - \text{sign}\{\omega_j - \omega_i - \omega_k\} \\ & \times \left[ \sqrt{\frac{aK_{ijk}^2}{8(2\pi c)^4 \omega_i \omega_j \omega_k} + \left| \frac{\omega_j - \omega_i - \omega_k}{2} \right|^2} \right. \\ & \left. - \left| \frac{\omega_j - \omega_i - \omega_k}{2} \right| \right] \left. \right\} \end{aligned} \quad (23)$$

Using  $\tilde{\mathcal{S}}_{ii}$  and  $\tilde{\mathcal{S}}_{ij}$ , eq 7 can be fully rewritten devoid of resonance terms:

$$\nu_i - \omega_i = 2\tilde{\mathcal{S}}_{ii} + 2\mathcal{N}_{ii} + 2\mathcal{T}_{ii} + \frac{1}{2} \sum_{i=1}^N [\tilde{\mathcal{S}}_{ij} + \mathcal{N}_{ij} + \mathcal{T}_{ij}] \quad (24)$$

While the expression given above offers the possibility of computing fundamental bands without concern for the risk of resonances, the conditions for which the DCPT2 approach is valid should be carefully defined, so that possible shortcomings are well identified. To this end, let us start from eq 19, assuming that both  $k$  and  $\varepsilon$  are positive, so that we can safely disregard the issue of the sign  $S$ . We reformulate it as a Taylor expansion up to the second order:

$$\lim_{k \rightarrow 0} (\sqrt{k^2 + \varepsilon^2}) = \varepsilon + \frac{k^2}{2\varepsilon}$$

Then, we note that if  $\varepsilon$  is small, VPT2 cannot be applied, and DCPT2 represents a more suitable model. Next, if  $\varepsilon$  is large, VPT2 obviously leads to correct results, but for all cases where  $k$  is small, DCPT2 tends to the same results as VPT2, so DCPT2 can also be safely used. Finally, if  $k$  is large, then DCPT2 deviates from VPT2; thus the latter must be preferred. With these considerations in mind, we introduce a mixed-scheme, hereafter called HDCPT2 and defined as

$$f_{\text{HDCPT2}} = \Lambda f_{\text{VPT2}} + (1 - \Lambda) f_{\text{DCPT2}} \quad (25)$$

where  $f_{\text{VPT2}}$  represents the value of a possibly resonant term in eq 17 or eq 18 calculated at the VPT2 level and  $f_{\text{DCPT2}}$  its counterpart calculated by means of DCPT2.  $\lambda$  is a scaling term, given by

$$\Lambda = \frac{\tanh(\alpha[\sqrt{k^2 \varepsilon^2} - \beta]) + 1}{2}$$

$\beta$  is the threshold to control the transition from DCPT2 to VPT2 depending on the value of  $k$  and  $\varepsilon$ , while  $\alpha$  controls the "smoothness" of the transition.

As an example, the second term of eq 18 at the HDCPT2 level is transformed as

$$\begin{aligned} & \frac{a}{4(2\pi c)^4 \omega_i \omega_j} \frac{K_{ij}^2}{\omega_j(2\omega_i - \omega_j)} \\ & \rightarrow \Lambda \left\{ \frac{aK_{ij}^2}{4(2\pi c)^4 \omega_i \omega_j^2 (2\omega_i - \omega_j)} \right\} + (1 - \Lambda) \\ & \times \left\{ \text{sign}\{2\omega_i - \omega_j\} \left[ \sqrt{\frac{aK_{ij}^2}{4(2\pi c)^4 \omega_i \omega_j^2} + \left| \frac{2\omega_i - \omega_j}{2} \right|^2} \right. \right. \\ & \left. \left. - \left| \frac{2\omega_i - \omega_j}{2} \right| \right] \right\} \end{aligned} \quad (26)$$

By generalizing the above transformation to all terms treated at the DCPT2 level, we obtain the final expression for the fundamental bands:

$$\nu_i - \omega_i = 2\tilde{S}_{ii}^{\Lambda} + 2N_{ii} + 2T_{ii} + \frac{1}{2} \sum_{\substack{i=1 \\ j \neq i}}^N [\tilde{S}_{ij}^{\Lambda} + N_{ij} + T_{ij}] \quad (27)$$

where the superscript  $\Lambda$  indicates that the term is calculated with the HDCPT2 model. From eq 4 and eq 27, it is possible to compute the vibrational partition function at the SPT level of theory (see eq 2) devoid of any singularity.

### 3. COMPUTATIONAL DETAILS

Density functional theory (DFT) has been employed to compute harmonic and anharmonic force fields. Within the DFT approach, the standard B3LYP functional<sup>72</sup> has been used in conjunction with the aug-N07D<sup>73</sup> basis set. Recently, the original polarized double- $\zeta$  basis set N07D<sup>73–76</sup> has been modified by consistent inclusion of diffuse  $s$  functions and then further augmented by one set of diffuse  $d$  functions on heavy atoms. On general grounds, the DFT/N07D approach has been developed for spectroscopic studies of medium-to-large molecular systems and provides an excellent compromise between reliability and computational effort.<sup>47,48,50,77,78</sup> Additionally, harmonic and anharmonic force fields have been computed using a double-hybrid functional (B2PLYP<sup>79</sup>) in conjunction with the aug-cc-pVTZ<sup>80,81</sup> basis set. In both cases, equilibrium structures have been optimized using tight convergence criteria, while the third ( $K_{ijk}$ ) and semidiagonal fourth ( $K_{ijij}$  and  $K_{iijk}$ ) force constants have been obtained by numerical differentiation of the analytical second derivatives (with the standard 0.01 Å step). Then, the semidiagonal quartic force fields have been used to compute anharmonic frequencies. Within the fully automated GVPT2 approach,<sup>20,21</sup> as implemented in the Gaussian package,<sup>23,24,32</sup> nearly resonant contributions are removed from the perturbative treatment (DVPT2 model) and then treated variationally.<sup>21,23</sup> The criteria to define Fermi resonances chosen in this work are those proposed by Martin et al.,<sup>25</sup> as they are known to provide accurate results.<sup>44,82</sup> DCPT2 and HDCPT2 approaches have been also implemented following the equations given in section 2. For HDCPT2 calculations, the parameters used to compute  $\lambda$  were  $\alpha = 1.0$  and  $\beta = 5.0 \times 10^5$ . Extensive tests have shown that  $\lambda$  has negligible sensitivity to those values, so rather large variations about them have little effect on the results.

A hybrid CCSD(T)/DFT approach<sup>42,48,52–55,83</sup> has also been applied to perturbative anharmonic computations. This model is based on the assumption that the differences between CCSD(T) and B3LYP results are mainly due to the harmonic terms. In this way, prohibitively expensive computations of cubic and quartic force constants at the CCSD(T) level are avoided, and the hybrid CCSD(T)/DFT scheme therefore provides a viable route to anharmonic computations for relatively large systems. The simplest hybrid model relies on *a posteriori* DFT corrections to the best estimated harmonic results. Such an approximation has already been validated for vibrational frequencies of several closed- and open-shell systems (see for instance refs 42, 48, 54, 55, and 83). In the second approach, improved harmonic frequencies are introduced directly into the VPT2 computations along with the

third and fourth force constants obtained at the DFT level. This model has been applied here to computations of vibrational partition functions and provides corrections to all properties in a fully automated manner. It is also noteworthy that, using the HDCPT2 model, the above two procedures lead to results much closer to each other than in the GVPT2 framework.

All computations have been performed employing a locally modified version of the Gaussian suite of programs for quantum chemistry.<sup>84</sup>

### 4. RESULTS AND DISCUSSIONS

**4.1. The Zero-Point Vibrational Energy.** Let us start with a discussion about the accuracy of zero-point vibrational energies computed using eq 4, which, as already mentioned, avoids the problem of singularities and is applicable also to transition states, thus allowing a consistent computation of smooth ZPVE-corrected reaction paths. In this respect, very accurate data for harmonic vibrational frequencies, anharmonic constants, and ZPVE have been derived from spectroscopic results for a large set of diatomic molecules.<sup>85</sup> For the purposes of the present work, we have chosen a set of closed- and open-shell diatomic molecules, considering only atoms from the first three rows of the periodic table. Table 1 compares theoretical data computed at the B3LYP/aug-N07D and B2PLYP/aug-cc-pVTZ levels with accurate experimental results.<sup>85</sup> Of course, the problem of resonances is not present for diatomic molecules, so that anharmonic frequencies computed with the standard VPT2 approach are reported. Additionally, *ad hoc* scaling factors for both frequencies and ZPVE have been estimated for each molecule. Concerning harmonic vibrational frequencies, we note that the B3LYP/aug-N07D values show a mean absolute error (MAE) with respect to experimental results lower than 50 cm<sup>−1</sup>, and a significant improvement is obtained with B2PLYP/aug-cc-pVTZ computations (MAE of 25 cm<sup>−1</sup>). On the contrary, both computational models predict very accurate anharmonic corrections with a MAE of 3 cm<sup>−1</sup> and largest deviations of about 10 cm<sup>−1</sup>. Such findings further strengthen the validity of hybrid computational models, where the harmonic part of the potential evaluated at a high level of theory is corrected for anharmonicity at the DFT level,<sup>48,54,55,83</sup> allowing accurate spectroscopic studies even for relatively large molecular systems. As far as ZPVE is concerned, the results presented in Table 1 clearly show that both computational approaches provide accurate theoretical data, with a MAE well below 0.5 kJ mol<sup>−1</sup> for the harmonic part and below 0.1 kJ mol<sup>−1</sup> for anharmonic correction, suggesting that anharmonic ZPVEs evaluated at the DFT level represent a viable route for the theoretical prediction of thermochemistry parameters. Additionally, it is shown that the experimentally determined ratio between harmonic and anharmonic ZPVE changes from 0.990 to 0.998, with even larger differences found for the theoretical estimates, 0.970–0.998 and 0.970–1.000 for B3LYP/aug-N07D and B2PLYP/aug-cc-pVTZ, respectively. Moreover, we note that both experimental and theoretical *ad hoc* scaling factors vary significantly when applied to the frequencies or to the ZPVE, with differences between averaged values of 0.012, 0.011, and 0.015 for B3LYP/aug-N07D, B2PLYP/aug-cc-pVTZ, and experimental results, respectively. On the contrary, the perturbative computations provide accurate anharmonic corrections for both frequencies and ZPVE. Thus, taking into account that VPT2 computations at the B3LYP/aug-N07D level are feasible for relatively large molecular systems, an anharmonic perturbative model leading

Table 1. Vibrational Frequencies [in  $\text{cm}^{-1}$ ] and Zero Point Vibrational Energies (ZPVE) [in  $\text{kJ mol}^{-1}$ ] Computed for the Benchmark Set Composed of Diatomic Closed- and Open-Shell Molecules<sup>a</sup>

molecule	frequencies						zero-point vibrational energies					
	B3LYP/aug-N07D			B2PLYP/aug-cc-pVTZ			B3LYP/aug-N07D			B2PLYP/aug-cc-pVTZ		
	$\omega_e$	$\omega_e^{\text{ZPE}}$	$\nu/\omega_e$	$\omega_e$	$\omega_e^{\text{ZPE}}$	$\nu/\omega_e$	Harm	Anh-Harm	Anh/Harm	Harm	Anh-Harm	Anh/Harm
CH	2829	60	0.957	2883	60	0.958	16.9	-0.28	0.984	17.2	-0.28	0.984
Cl <sub>2</sub>	535	2	0.991	552	2	0.993	3.2	-0.01	0.997	3.3	-0.01	0.998
ClF	773	4	0.990	786	4	0.989	4.6	-0.02	0.987	4.7	-0.02	0.996
ClO	839	5	0.988	872	5	0.989	5.0	-0.02	0.987	5.2	-0.02	0.996
CN	2147	13	0.988	2075	2	0.998	12.8	-0.05	0.996	12.4	0.00	1.000
CO	2207	13	0.988	2154	14	0.987	13.2	-0.05	0.996	12.9	-0.06	0.996
F <sub>2</sub>	1024	7	0.986	1016	8	0.984	6.1	-0.03	0.996	6.1	-0.03	0.995
H <sub>2</sub>	4427	118	0.947	4464	117	0.948	26.5	-0.79	0.970	26.7	-0.79	0.970
HCl	2946	45	0.970	2986	44	0.971	17.6	-0.19	0.989	17.9	-0.19	0.990
HF	4069	88	0.957	4099	86	0.958	24.3	-0.40	0.984	24.5	-0.40	0.984
LiH	1393	20	0.971	1424	24	0.967	8.3	-0.11	0.987	8.5	-0.13	0.985
N <sub>2</sub>	2452	13	0.989	2341	15	0.987	14.7	-0.06	0.996	14.0	-0.06	0.995
NH	3263	71	0.956	3313	72	0.957	19.5	-0.32	0.984	19.8	-0.33	0.983
NO	1983	13	0.987	1891	12	0.987	11.9	-0.05	0.996	11.3	-0.04	0.996
O <sub>2</sub>	1648	10	0.988	1530	13	0.984	9.9	-0.04	0.996	9.2	-0.05	0.995
OH	3708	76	0.959	3736	76	0.959	22.2	-0.34	0.985	22.3	-0.35	0.984
S <sub>2</sub>	702	2	0.993	704	3	0.992	4.2	-0.01	0.998	4.2	-0.01	0.998
SH	2662	48	0.964	2707	49	0.964	15.9	-0.21	0.987	16.2	-0.23	0.986
SO	1104	5	0.990	1115	7	0.988	6.6	-0.02	0.997	6.7	-0.03	0.996
MIN <sup>c</sup>	-69	-9	-0.030 <sup>e</sup>	-50	-11	-0.029 <sup>e</sup>	-0.4	-0.5	-0.019 <sup>f</sup>	-0.3	-0.5	-0.018 <sup>f</sup>
MAX <sup>c</sup>	107	0	0.016 <sup>e</sup>	99	1	0.021 <sup>e</sup>	0.6	0.0	0.009 <sup>f</sup>	0.6	0.0	0.012 <sup>f</sup>
MAE <sup>d</sup>	45	3	0.014 <sup>e</sup>	25	3	0.014 <sup>e</sup>	0.3	0.1	0.006 <sup>f</sup>	0.2	0.1	0.007 <sup>f</sup>

<sup>a</sup>The harmonic frequencies  $\omega_e$ , anharmonic contributions  $\omega_e^{\text{ZPE}}$ , and the ratio  $\nu/\omega_e$  are reported. For ZPVE harmonic values (Harm), the anharmonic contribution to the ZPVE (Anh-Harm) and the ratio between ZPVE<sup>anh</sup> and ZPVE<sup>harm</sup> (Anh/Harm) are listed. All computations have been performed at the B3LYP/aug-N07D and B2PLYP/aug-cc-pVTZ levels of theory, and results are compared to the accurate experimental data. <sup>b</sup>Experimental data from ref 85. <sup>c</sup>MIN and MAX stands for signed errors, largest positive (MAX) and largest negative (MIN). See text. <sup>d</sup>MAE stands for Mean Absolute Error. See text. <sup>e</sup>Computed with respect to average scaling factor estimated on the basis of the data reported in this table: 0.977 for B3LYP/aug-N07D, 0.977 for B2PLYP/aug-cc-pVTZ, and 0.974 for experimental data. <sup>f</sup>Computed with respect to average scaling factor estimated on the basis of the reference data from Tables 1–3: 0.989 for B3LYP/aug-N07D, 0.988 for B2PLYP/aug-cc-pVTZ, and 0.989 for experimental data.

Table 2. Zero-Point Vibrational Energies (ZPVE) in  $\text{kJ mol}^{-1}$  Computed for the Benchmark Set Composed of Small Closed- and Open-Shell Molecules<sup>a</sup>

ZPE [kJ/mol]	B3LYP/aug-N07D				B2PLYP/aug-cc-pVTZ				best estimates <sup>b</sup>				$\Delta^{\text{best}}(\text{Harm})$				$\Delta^{\text{best}}(\text{Anh-Harm})$			
	Harm	Anh	Anh-Harm	Anh/Harm	Harm	Anh	Anh-Harm	Anh/Harm	Harm	Anh	Anh-Harm	Anh/Harm	B3LYP	B2PLYP	B3LYP	B2PLYP	B3LYP	B2PLYP	B3LYP	B2PLYP
	B3LYP/aug-N07D				B2PLYP/aug-cc-pVTZ				best estimates <sup>b</sup>				$\Delta^{\text{best}}(\text{Harm})$				$\Delta^{\text{best}}(\text{Anh-Harm})$			
NH <sub>2</sub>	49.9	49.1	-0.8	0.984	50.4	49.6	-0.8	0.984	50.2	49.3	-0.9	0.982	-0.3	0.2	-0.3	0.1	0.1	0.1	0.1	0.1
H <sub>2</sub> O	56.0	55.2	-0.9	0.984	56.1	55.2	-0.9	0.984	56.4	55.5	-0.9	0.984	-0.4	-0.3	-0.4	0.0	0.0	0.0	0.0	0.0
H <sub>2</sub> S	39.4	38.9	-0.5	0.987	39.9	39.4	-0.5	0.987	39.9	39.3	-0.6	0.985	-0.5	0.0	-0.5	0.1	0.1	0.1	0.1	0.1
SO <sub>2</sub>	17.0	16.9	-0.1	0.996	17.5	17.4	-0.1	0.996	18.4	18.3	-0.1	0.995	-1.4	-0.9	-1.4	0.0	0.0	0.0	0.0	0.0
HOCl	34.4	33.9	-0.5	0.987	34.6	34.1	-0.5	0.986	34.7	34.2	-0.5	0.986	-0.3	-0.1	-0.3	0.0	0.0	0.0	0.0	0.0
HOF	36.5	36.0	-0.5	0.986	36.5	36.0	-0.5	0.986	36.6	36.0	-0.6	0.984	-0.1	-0.1	-0.1	0.1	0.1	0.1	0.1	0.1
CH <sub>3</sub> Cl	98.8	98.2	-0.6	0.994	99.8	98.4	-1.4	0.986	99.7 <sup>c</sup>	98.9 <sup>c</sup>	-0.8	0.992	-0.9	0.1	-0.9	0.2	-0.6	-0.6	-0.6	-0.6
SSH	28.5	28.3	-0.1	0.996	29.1	28.8	-0.3	0.989	28.7 <sup>d</sup>	28.0 <sup>d</sup>	-0.7	0.977	-0.2	0.5	-0.2	0.5	0.3	0.3	0.3	0.3
NO <sub>2</sub>	23.2	23.0	-0.2	0.992	22.6	22.5	-0.1	0.994	22.8 <sup>e</sup>	22.5 <sup>e</sup>	-0.3	0.988	0.4	-0.1	0.1	0.1	0.2	0.2	0.2	0.2
HCO	34.0	33.4	-0.7	0.981	34.1	33.5	-0.7	0.981	34.9	34.0	-0.9	0.974	-0.9	-0.8	-0.9	0.2	0.2	0.2	0.2	0.2
FNO	19.4	19.3	-0.1	0.996	18.9	18.8	-0.1	0.995	19.0	18.9	-0.1	0.995	0.4	-0.1	0.0	0.0	0.0	0.0	0.0	0.0
CINO	17.2	17.1	-0.1	0.995	16.7	16.6	-0.1	0.994	16.7	16.6	-0.1	0.994	0.5	0.0	0.0	0.0	0.0	0.0	0.0	0.0
F <sub>2</sub> O	14.1	14.0	-0.1	0.995	14.0	14.0	-0.1	0.994	13.7	13.6	-0.1	0.993	0.4	0.3	0.0	0.0	0.0	0.0	0.0	0.0
ClO <sub>2</sub>	13.5	13.5	-0.1	0.995	14.4	14.4	0.0	0.997	15.2	15.1	-0.1	0.993	-1.7	-0.8	-1.7	0.0	0.1	0.1	0.1	0.1
H <sub>2</sub> SiO	47.4	46.9	-0.5	0.990	48.5	48.0	-0.5	0.990	48.7	48.2	-0.5	0.990	-1.3	-0.2	-1.3	0.0	0.0	0.0	0.0	0.0
<i>trans</i> -HSiOH	54.1	53.3	-0.8	0.986	54.8	54.0	-0.8	0.985	55.0	54.2	-0.8	0.985	-0.9	-0.2	-0.9	0.0	0.0	0.0	0.0	0.0
N <sub>2</sub> H <sub>2</sub>	74.4	73.2	-1.2	0.983	74.6	73.3	-1.3	0.983	74.4	73.2	-1.2	0.984	0.0	0.2	0.0	0.0	-0.1	-0.1	-0.1	-0.1
CH <sub>2</sub> F <sub>2</sub>	85.5	84.4	-1.1	0.987	86.5	85.4	-1.1	0.988	86.5	85.5	-1.0	0.988	-1.0	0.0	-1.0	0.0	-0.1	-0.1	-0.1	-0.1
H <sub>2</sub> CO	69.6	68.6	-0.9	0.987	70.0	69.1	-0.9	0.987	70.4	69.2	-1.2	0.983	-0.8	-0.4	-0.8	0.3	0.3	0.3	0.3	0.3
C <sub>2</sub> H <sub>4</sub>	133.5	131.7	-1.8	0.987	134.3	132.8	-1.5	0.989	133.4	131.7	-1.7	0.987	0.1	0.9	-0.1	0.2	0.2	0.2	0.2	0.2
HCOOH	85.2	84.1	-1.1	0.988	88.6	87.4	-1.2	0.986	86.2	85.2	-1.0	0.988	-1.0	2.4	-1.0	-0.2	-0.2	-0.2	-0.2	-0.2
NH <sub>3</sub>	90.1	88.6	-1.5	0.983	90.4	88.8	-1.5	0.983	90.7 <sup>f</sup>	88.7 <sup>g</sup>	-1.9	0.979	-0.6	-0.3	-0.6	0.4	0.4	0.4	0.4	0.4
H <sub>2</sub> CS	64.7	63.8	-0.9	0.987	65.1	64.2	-0.8	0.987	64.8	63.8	-1.0	0.985	-0.1	0.3	-0.1	0.1	0.2	0.2	0.2	0.2
<i>cis</i> -HSiOH	53.1	52.3	-0.8	0.985	53.8	53.0	-0.8	0.985	54.0	53.2	-0.8	0.985	-0.9	-0.2	-0.9	0.0	0.0	0.0	0.0	0.0
CH <sub>3</sub> NH	104.5	103.0	-1.5	0.985	105.0	103.5	-1.5	0.986	104.7	103.2	-1.5	0.986	-0.2	0.3	-0.2	0.0	0.0	0.0	0.0	0.0
CHO-CHO	96.7	95.6	-1.1	0.989	97.1	95.9	-1.1	0.988	98.4	97.3	-1.1	0.989	-1.7	-1.3	-1.7	0.0	0.0	0.0	0.0	0.0
MIN <sup>h</sup>				-0.009 <sup>j</sup>				-0.008 <sup>j</sup>				-0.015 <sup>j</sup>					-0.1	-0.1	-0.6	-0.6
MAX <sup>h</sup>				0.007 <sup>j</sup>				0.009 <sup>j</sup>				0.005 <sup>j</sup>					0.5	0.5	0.4	0.4
MAE <sup>i</sup>				0.004 <sup>j</sup>				0.004 <sup>j</sup>				0.005 <sup>j</sup>					0.7	0.4	0.1	0.1

<sup>a</sup>Harmonic (Harm) and total anharmonic (Anh) ZPVE are listed along with the anharmonic contribution to the ZPVE (Anh-Harm) and the ratio between ZPVE<sup>Anh</sup> and ZPVE<sup>Harm</sup> (Anh/Harm). All ZPVE computations have been performed at the B3LYP/aug-N07D and B2PLYP/aug-cc-pVTZ levels of theory and compared to the best available theoretical or experimental results. <sup>b</sup>Reference data based on high level harmonic and anharmonic force fields. For H<sub>2</sub>O, H<sub>2</sub>S, HCO, H<sub>2</sub>CO, CH<sub>3</sub>F<sub>2</sub> and C<sub>2</sub>H<sub>4</sub>, experimental force fields; for NH<sub>3</sub>, SO<sub>2</sub>, HOCl, HOF, FNO, ClNO, F<sub>2</sub>O, ClO<sub>2</sub>, H<sub>2</sub>SiO, N<sub>2</sub>H<sub>2</sub>, CH<sub>2</sub>F<sub>2</sub>, HCOOH, H<sub>2</sub>CS, *cis*-HSiOH, CH<sub>3</sub>NH, CHO-CHO, theoretical force fields obtained at, at least, CCSD(T)/cc-pVTZ level. See ref 24 for the details. <sup>c</sup>Estimated in ref 7 based on the experimental force field from ref 112. <sup>d</sup>Best theoretical estimates based on the data from ref 86 and computed as CCSD(T)/(6-31G\*\*+(MP2/6-311G(2dfp)-MP2/6-31G\*\*)). <sup>e</sup>From vibrational computations in ref 87 based on the empirical PES from ref 113. <sup>f</sup>From harmonic frequency computations at CCSD(T)/cc-pwCVQZ level. <sup>g</sup>From variational computations<sup>89</sup> with an exact kinetic energy operator based on six-dimensional PES obtained from CCSD(T)/aug-cc-pVQC and CCSD(T)/aug-cc-pVTZ computations, with subsequent fitting of the  $V_0$  term to experimental values of <sup>14</sup>NH<sub>3</sub>. <sup>h</sup>MIN and MAX stand for signed errors, largest positive (MAX) and largest negative (MIN). See text. <sup>i</sup>MAE stands for Mean Absolute Error. See text. <sup>j</sup>Computed with respect to average scaling factor estimated on the basis of the reference data from Tables 1–3; 0.989 for B3LYP/aug-N07D, 0.988 for B2PLYP/aug-cc-pVTZ, and 0.989 for experimental data.



Table 3. Zero-Point Vibrational Energies (ZPVE) in  $\text{kJ mol}^{-1}$  Computed for Small- and Medium-Sized Molecules at the B3LYP/aug-N07D Level<sup>a</sup>

molecule	B3LYP/aug - N07D				comp. <sup>b</sup>		exp. <sup>c</sup>		best estimates	
	Harm	Anh	Anh/Harm	Fund	Harm	Fund			comp. corr. <sup>d</sup>	exptl. corr. <sup>e</sup>
H <sub>2</sub> O	56.0	55.2	0.984	53.6	56.4	53.9			55.5	55.5
H <sub>2</sub> S	39.4	38.9	0.987	38.0	39.9	38.4			39.4	39.3
HCO	34.0	33.4	0.981	32.2	34.9	32.2			34.2	33.4
SO <sub>2</sub>	17.0	16.9	0.996	16.8	18.4	18.1			18.3	18.2
H <sub>2</sub> CO	69.6	68.6	0.987	67.0	70.4	67.5			69.5	69.2
C <sub>2</sub> H <sub>4</sub>	133.5	131.7	0.987	128.8	133.4	129.0			131.6	131.9
CH <sub>2</sub> F <sub>2</sub>	85.5	84.4	0.987	82.7	86.5	84.2			85.4	85.8
NH <sub>2</sub>	49.9	49.1	0.984	47.7	50.2	47.9			49.4	49.4
HOCl	34.4	33.9	0.987	33.1	34.7	33.3			34.2	34.2
F <sub>2</sub> O	14.1	14.0	0.995	13.9	13.7	13.3			13.6	13.4
ClNO	17.2	17.1	0.995	17.0	16.7	16.3			16.6	16.5
CH <sub>3</sub> CHO	144.8	142.9	0.987	139.8	146.0 <sup>f</sup>	140.4			144.1	143.5
acrolein	160.5	158.5	0.988	155.6	160.4 <sup>g</sup>	155.6 <sup>h</sup>			158.4	158.5
glycine	208.8	206.2	0.987	201.6	209.7 <sup>f</sup>	202.5 <sup>i</sup>			207.1	207.0
thiophene	174.4	172.6	0.989	169.6	174.5 <sup>j</sup>	169.9 <sup>k</sup>			172.6	172.9
furan	183.1	181.1	0.989	177.9	183.3 <sup>l</sup>	178.5 <sup>m</sup>			181.2	181.6
malonaldehyde	177.4	174.6	0.984	168.8	177.7 <sup>n</sup>	168.7 <sup>o</sup>			174.9	174.4
pyrimidine	201.8	199.5	0.989	196.0	202.5 <sup>f</sup>	196.0 <sup>p</sup>			200.2	199.5
pyridine	232.5	229.7	0.988	225.8	233.5 <sup>f</sup>	225.8 <sup>q</sup>			230.7	229.8
uracil	228.1	225.6	0.989	221.7	228.2 <sup>r</sup>	222.8 <sup>s</sup>			225.7	226.7
MIN <sup>t</sup>		−1.47							−1.01	
MAX <sup>t</sup>		0.63							0.88	
MAE <sup>t</sup>		0.51							0.35	

<sup>a</sup>Harmonic (Harm) and total anharmonic (Anh) ZPVE are listed along with the ratio between ZPVE<sup>Anh</sup> and ZPVE<sup>Harm</sup> (Anh/Harm) and the “Fundamentals” ZPVE (Fund). Additionally, the best estimated values obtained by correcting the harmonic ZPVE with computations at a higher level of theory, or applying an empirical scheme based on the comparison between computed and experimental “Fundamentals” ZPVE are reported. <sup>b</sup>See Table 2 “Fundamentals” ZPVE as reported in ref 94. <sup>c</sup>Best theoretical estimates computed on the basis of the harmonic ZPVE reported in column five and the anharmonic contribution evaluated at the B3LYP/aug-N07D level, see text for details. <sup>d</sup>Best empirical estimates based on the anharmonic ZPVE computed at the B3LYP/aug-N07D level and correction for the harmonic part evaluated as a difference between computed and experimental “Fundamentals” ZPVE, see text for details. <sup>e</sup>Computed at the B2PLYP/aug-cc-pVTZ level, this work. <sup>f</sup>Harmonic computations at the CCSD(T)/cc-pVTZ level from ref 90. <sup>g</sup>Experimental frequencies from ref 114. <sup>h</sup>Experimental frequencies from ref 106, except for the  $\nu_{\text{OH}}$  from ref 115. <sup>i</sup>Harmonic computations at the CCSD(T)/cc-pV(T+d)Z level from ref 91. <sup>j</sup>Experimental frequencies from ref 116. <sup>k</sup>Harmonic computations at the CCSD(T)/cc-pVTZ level from ref 92. <sup>l</sup>Experimental frequencies from ref 117. <sup>m</sup>Harmonic computations at the CCSD(T)/aug-cc-pVTZ level from ref 93. <sup>n</sup>Experimental frequencies from refs 118 and 119 as compiled in ref 120. <sup>p</sup>Experimental frequencies from ref 110. <sup>q</sup>Experimental frequencies from ref 121. <sup>r</sup>Best estimate from the composite scheme CCSD(T)+CV/CBS, see ref 83 for details. <sup>s</sup>Experimental frequencies from refs 107–109. <sup>t</sup>MIN and MAX stands for signed errors, largest positive (MAX) and largest negative (MIN). MAE stands for Mean Absolute Error. Errors with respect to the experimentally corrected best value.

to consistent corrections for both frequencies and ZPVE can be recommended over schemes employing often ambiguous scaling factors. Although generation of an anharmonic PES is, of course, much more expensive than for its harmonic counterpart, effective reduced-dimension approaches can be used to take into account only a subset of normal modes.<sup>77</sup>

Further insights into the accuracy of zero-point vibrational energies computed in the present work can be gained by comparison with the best estimates based on accurate experimental or theoretical harmonic and anharmonic force fields. To this aim, we resort to a benchmark set containing several closed- and open-shell small molecules (H<sub>2</sub>O, H<sub>2</sub>S, HCO, H<sub>2</sub>CO, CH<sub>2</sub>F<sub>2</sub>, C<sub>2</sub>H<sub>4</sub>, NH<sub>2</sub>, SO<sub>2</sub>, HOCl, HOF, FNO, ClNO, F<sub>2</sub>O, ClO<sub>2</sub>, H<sub>2</sub>SiO, N<sub>2</sub>H<sub>2</sub>, CH<sub>2</sub>F<sub>2</sub>, HCOOH, H<sub>2</sub>CS, *cis*-HSiOH, CH<sub>2</sub>NH, and CHO–CHO) reported in a previous work by one of the present authors,<sup>24</sup> extended by a few others for which accurate ZPVEs have been reported more recently (CH<sub>3</sub>Cl,<sup>7</sup> SSSH,<sup>86</sup> NO<sub>2</sub>,<sup>87</sup> NH<sub>3</sub><sup>88,89</sup>). Comparison between harmonic ZPVE and anharmonic contributions computed at the B3LYP/aug-N07D and B2PLYP/aug-cc-pVTZ levels and

the reference data is reported in Table 2. It is evident that the largest discrepancies between ZPVE computed at the DFT level are related to the harmonic contributions, with the B2PLYP/aug-cc-pVTZ results nearly halving the mean average error with respect to B3LYP/aug-N07D. Moreover, as already observed for the diatomic molecules, both DFT approaches provide similar anharmonic corrections, which, in turn, agree with the best results within 0.1  $\text{kJ mol}^{-1}$ . Additionally, it is again evident that the ratio between the total anharmonic ZPVE and its harmonic counterpart varies significantly for different molecules, strengthening the conclusions based on the analysis of diatomic molecules. The results reported in Tables 1 and 2 show that computations of anharmonic ZPVEs using eq 4 and B3LYP/aug-N07D yield results valuable for thermochemical studies, and further improvements are possible by correcting the harmonic ZPVE component, e.g., at the coupled-cluster or B2PLYP/aug-cc-pVTZ levels. Such a hybrid strategy has been employed to evaluate anharmonic ZPVEs for several medium-size molecules (acrolein, glycine, thiophene, furan, malonaldehyde, pyrimidine, pyridine, uracil, and toluene), with harmonic

ZPVEs corrected by the available CCSD(T) results,<sup>83,90–93</sup> or computed at the B2PLYP/aug-cc-pVTZ level in the present work. Additionally, an empirical scheme proposed by Perdew et al.<sup>94</sup> and based on the correction to the harmonic ZPVE by comparison between theoretical and experimental “Fundamentals” ZPVE (computed as  $1/2\sum\nu_i$ ) has been considered. This approach is based on the assumption that the difference between theoretical and experimental “Fundamentals” ZPVE ( $ZPVE_{\text{Fund}}$ ) is mainly due to the harmonic part, so that  $\Delta(ZPVE_{\text{Fund}}^{\text{Comp.}} - ZPVE_{\text{Fund}}^{\text{Exp.}})$  can be used to correct the harmonic ZPVE component. The benchmark data reported in Tables 1 and 2 further validate this simple approach. In Table 3, both schemes to estimate accurate anharmonic ZPVEs are applied to medium-sized molecules, and additionally to a few smaller ones, in order to provide a more complete comparison between the two hybrid models. The anharmonic B3LYP/aug-N07D fundamentals used to obtain  $ZPVE_{\text{Fund}}^{\text{Comp.}}$  have been computed with the HDCPT2 model. Our results clearly show that both hybrid approaches lead in most cases to very similar results, with an average discrepancy of less than  $0.5 \text{ kJ}\cdot\text{mol}^{-1}$ ; thus both models can be recommended as viable routes to estimate accurate ZPVEs. It should be also noted that computations of anharmonic ZPVEs at the B3LYP/aug-N07D level, employing eq 4, already provide reliable results with a MAE of about  $0.5 \text{ kJ}\cdot\text{mol}^{-1}$  with respect to both hybrid approaches. On the grounds of the above analysis, we suggest that perturbative anharmonic computation of ZPVEs, which at the DFT level is feasible even for large molecular systems, should be considered as a more reliable route with respect to schemes based on the simple scaling of the harmonic ZPVEs, even if the latter are computed at higher levels of theory.

**4.2. The Vibrational Partition Function and Thermodynamical Properties.** A fully black-box procedure requires that vibrational partition functions remain consistent along reaction paths and that results from different computational models be coherent. To this end, a general approach to compute zero-point energies according to eq 4 needs to be followed by a robust procedure to compute vibrational frequencies free from possible discontinuities related to diverse definitions of resonance interactions. As discussed in section 2, the HDCPT2 model takes advantage from the degeneracy-corrected second-order perturbation theory, allowing also to avoid problems related to the accuracy of the Taylor expansion used in the DCPT2 treatment. Here, we report, as an example, toluene (see Table 4), for which a very strong coupling between low- and high-frequency vibrations of the methyl group, namely, the  $\text{CH}_3$  rotation ( $\nu_{39}$ ) and the symmetric C–H stretching ( $\nu_8$ ), is observed and leads to unphysical DCPT2 results for the frequencies of these modes (please note that for rotation motion, Table 4 reports the result obtained by the one-dimensional Hindered Internal Rotation (HR) Model<sup>95–97</sup>). On the contrary, the problem is fully overcome with the HDCPT2 model, which, in fact, leads to frequencies in very good agreement with the GVPT2 reference (average absolute deviation of  $3 \text{ cm}^{-1}$ , and difference lower than  $20 \text{ cm}^{-1}$  for the problematic  $\nu_8$  mode). Next, anharmonic real frequencies for global minimum and transition state structures of malonaldehyde computed with the GVPT2, VPT2, DCPT2, and HDCPT2 models are reported in Table 5. The simple VPT2 model leads to absolute discrepancies with respect to the GVPT2 reference as large as  $82 \text{ cm}^{-1}$  and  $209 \text{ cm}^{-1}$  for the minimum and the transition state, respectively. On the contrary, both

deperturbed models provide results in very good agreement with GVPT2, for both stationary points (average errors and maximum discrepancies lower than  $4 \text{ cm}^{-1}$  and  $45 \text{ cm}^{-1}$ , respectively), supporting the suitability of the HDCPT2 approach to obtain consistent vibrational frequencies along reaction paths.

Thus, all ingredients necessary to define a general approach to evaluate the degeneracy-corrected vibrational partition function  $\tilde{Q}_{\text{vib}}$  beyond the harmonic approximation are provided by zero-point energies obtained according to eq 4, anharmonic vibrational computations by means of the HDCPT2 model in conjunction with simple perturbation theory<sup>56</sup> rewritten for the general case in eq 2.  $\tilde{Q}_{\text{vib}}$  can then be used to obtain analytical expressions for the vibrational contributions to the internal energy ( $U$ ), entropy ( $S$ ), and constant volume specific heat ( $c_n$ ):<sup>24</sup>

$$U_n = R \frac{E_0}{k_B} + R \sum_{i=1}^{N_R} \frac{hc\nu_i/k_B}{e^{hc\nu_i/(k_B T)} - 1} \quad (28)$$

$$S_n = R \sum_{i=1}^{N_R} \left[ \frac{hc\nu_i/(k_B T)}{e^{hc\nu_i/(k_B T)} - 1} - \ln(1 - e^{-hc\nu_i/(k_B T)}) \right] \quad (29)$$

$$c_n = R \sum_{i=1}^{N_R} e^{hc\nu_i/(k_B T)} \left[ \frac{hc\nu_i/(k_B T)}{e^{hc\nu_i/(k_B T)} - 1} \right]^2 \quad (30)$$

where  $R$  is the universal gas constant. From these state functions, enthalpies and free energies can be also derived.

We first present vibrational partition functions obtained over a broad range of temperatures for  $\text{H}_2\text{O}$  using the GVPT2, DCPT2, and HDCPT2 models and the force field generated at the B3LYP/aug-N07D and B2PLYP/aug-cc-pVTZ levels and hybrid CCSD(T)/CBS//B3LYP/aug-N07D approaches. The results are compared to other theoretical data including accurate estimates based on experimentally derived force fields in Table 6. It is apparent that all of the computational models considered lead to equivalent results over the whole range of temperatures. Additionally, comparison between DFT and hybrid models clearly shows that the discrepancies between DFT results and the best theoretical estimates should be attributed to the harmonic part. As a matter of fact, the fully *ab initio* CC/DFT results based on the SPT model agree very well with accurate computations involving the experimentally derived Hoy–Mills–Stray (HMS) quartic general force field.<sup>98</sup> Additional insights on the quality and applicability of our approach can be obtained by comparison of  $\tilde{Q}_{\text{vib}}$  computed using VPT2, GVPT2, DCPT2, and HDCPT2 models for larger molecules. For this purpose, the different vibrational partition functions (relative to the GVPT2 reference) have been plotted for glycine, uracil, and pyrimidine over the 0–2000 K temperature range in Figure 2. It should be noted that anharmonic contributions of low-frequency vibrations, which are not reproduced correctly by perturbation theory, should be excluded from such an analysis. In the case of hindered rotations, it is then possible to apply *a posteriori* corrections based on reliable interpolation equations between free rotor and harmonic oscillators limits.<sup>95–97,99–102</sup> This approach has been applied to evaluate  $\tilde{Q}_{\text{vib}}$  of glycine and entropies for molecules with one or two soft dihedral angles (*vide infra*). The results

**Table 4.** Anharmonic Frequencies (in  $\text{cm}^{-1}$ ) for Toluene Computed with the GVPT2, VPT2, DCPT2, and HDCPT2 Approaches Using the Force Field Generated at the B3LYP/aug-N07D Level<sup>a</sup>

mode	$\omega$	GVPT2			VPT2			DCPT2			HDCPT2		
		$\nu$	$\Delta_{\text{anh}}$		$\nu$	$\Delta_{\text{anh}}$	$\Delta_{\text{GVPT2}}$	$\nu$	$\Delta_{\text{anh}}$	$\Delta_{\text{GVPT2}}$	$\nu$	$\Delta_{\text{anh}}$	$\Delta_{\text{GVPT2}}$
1	3193	3055	(1)	−138	3064	−129	9	3062	−131	7	3062	−131	7
2	3180	3047	(11)	−134	3073	−108	26	3067	−113	21	3067	−113	21
3	3172	3044		−128	3044	−128	0	3044	−128	0	3044	−128	−1
4	3159	3029	(1)	−130	3041	−118	12	3034	−125	5	3034	−125	5
5	3158	3007	(16)	−151	2981	−177	−26	3005	−153	−1	3005	−153	−1
6	3107	2955	(−1)	−152	2993	−114	38	2921	−187	−34	2961	−147	6
7	3080	2935		−145	2935	−145	0	2705	−375	−229	2908	−172	−27
8	3022	2935	(−39)	−87	2928	−94	−7	−4406	−	−	2917	−105	−18
9	1649	1608		−41	1608	−41	0	1608	−41	0	1608	−41	0
10	1626	1586		−40	1586	−40	0	1587	−39	0	1587	−39	0
11	1529	1495		−34	1495	−34	0	1495	−34	0	1495	−34	0
12	1500	1462	(0)	−38	1445	−55	−17	1462	−38	0	1462	−38	0
13	1485	1442	(0)	−43	1432	−54	−11	1473	−12	31	1435	−50	−7
14	1467	1432	(2)	−35	1431	−37	−1	1441	−26	9	1441	−26	9
15	1411	1377		−34	1377	−34	0	1264	−147	−113	1376	−36	−1
16	1356	1336	(−4)	−20	1337	−19	1	1336	−20	0	1336	−20	0
17	1340	1316	(−7)	−24	1333	−7	17	1320	−20	4	1320	−20	4
18	1229	1202		−27	1202	−27	0	1202	−27	0	1202	−27	0
19	1202	1187		−15	1187	−15	0	1186	−16	0	1186	−16	0
20	1179	1166		−13	1166	−13	0	1166	−13	0	1166	−13	0
21	1109	1084	(7)	−24	1086	−23	2	1087	−21	3	1087	−21	3
22	1060	1033	(−1)	−28	1038	−22	6	1042	−18	10	1042	−18	10
23	1049	1032		−17	1032	−17	0	1032	−17	0	1032	−17	0
24	1015	1002	(0)	−13	981	−34	−21	995	−20	−7	995	−20	−7
25	1002	976		−25	976	−25	0	976	−25	0	976	−25	0
26	997	977		−20	977	−20	0	980	−17	3	980	−17	3
27	983	963		−20	963	−20	0	963	−20	0	963	−20	0
28	913	892		−21	892	−21	0	892	−21	0	892	−21	0
29	858	837		−20	837	−20	0	837	−20	0	837	−20	0
30	797	784		−13	784	−13	0	784	−13	0	784	−13	0
31	746	730		−16	730	−16	0	730	−16	0	730	−16	0
32	714	696		−18	696	−18	0	696	−18	0	696	−18	0
33	633	628		−5	628	−5	0	627	−5	0	627	−5	0
34	526	522		−4	522	−4	0	522	−4	0	522	−4	0
35	478	469		−9	469	−9	0	470	−9	0	470	−9	0
36	415	405		−10	405	−10	0	405	−10	0	405	−10	0
37	343	344		2	344	2	0	344	2	0	344	2	0
38	208	194	(−4)	−14	208	0	14	205	−3	12	205	−3	12
39 <sup>b</sup>	21	33		12	33	12	0	33	12	0	33	12	0
MAE <sup>c</sup>							5			13			3

<sup>a</sup>For GVPT2, the difference between deperturbed and variational values for modes involved in Fermi resonances is reported in parentheses.  $\Delta_{\text{GVPT2}}$  refers to the difference in the anharmonic correction with respect to the GVPT2 model. <sup>b</sup>Anharmonic frequency from Hindered Internal Rotation model.<sup>95–97</sup> <sup>c</sup>Mean Absolute Error (MAE) computed excluding strongly coupled modes 8 and 39.

presented in Figure 2 show that for low temperatures the vibrational partition functions computed with different approaches are very close, as the main factor is the zero-point vibrational energy, which, in all cases, has been computed with the same model (eq 4). Some differences are observed for higher temperatures. However, HDCPT2 computations always provide vibrational partition function within 5% from the GVPT2 value, even at high temperatures and in difficult cases with several Fermi resonances or strong couplings between low- and high-frequency modes (*vide infra*).

Comparison between computed and experimental entropies presented in Table 7 shows that for small molecules the harmonic approximation leads to discrepancies as large as 0.5

and 1.5  $\text{J mol}^{-1} \text{K}^{-1}$  for molecules without and with hindered internal rotations, respectively. Then, anharmonic corrections (including the hindered rotor contribution) improve the accuracy to about 0.2 and 0.5  $\text{J mol}^{-1} \text{K}^{-1}$ , respectively. Considering a medium-sized semirigid molecule (pyridine), the enthalpy computed at the harmonic level overestimates the experimental value by about 1.3  $\text{J mol}^{-1} \text{K}^{-1}$ , while inclusion of anharmonic corrections leads to an agreement with experimental results within 0.35  $\text{J mol}^{-1} \text{K}^{-1}$ . The largest discrepancy of the harmonic entropy with respect to experimental results (17.4  $\text{J mol}^{-1} \text{K}^{-1}$ ) is obtained for toluene and is reduced to about 6.5  $\text{J mol}^{-1} \text{K}^{-1}$  by a mixed approach in which the anharmonic perturbative computations are coupled with the correction obtained by the HR model.

Table 5. Anharmonic Real Frequencies (in  $\text{cm}^{-1}$ ) for Minimum and Transition State Structures of Malonaldehyde Computed by GVPT2, VPT2, DCPT2, and HDCPT2 Approaches Using the Force Field Generated at the B3LYP/aug-N07D Level<sup>a</sup>

mode <sup>b</sup>	$\omega$	GVPT2			VPT2			DCPT2			HDCPT2		
		$\nu$		$\Delta_{\text{anh}}$	$\nu$	$\Delta_{\text{anh}}$	$\Delta_{\text{GVPT2}}$	$\nu$	$\Delta_{\text{anh}}$	$\Delta_{\text{GVPT2}}$	$\nu$	$\Delta_{\text{anh}}$	$\Delta_{\text{GVPT2}}$
MIN													
1	3221	3093		−128	3093	−128	0	3091	−130	−2	3091	−130	−2
2	3178	3001	(−5)	−177	3083	−95	82	3025	−153	24	3025	−153	24
3	3092	2569	(−4)	−522	2550	−542	−20	2565	−526	−4	2565	−526	−4
4	2980	2811	(−6)	−169	2799	−182	−13	2806	−174	−5	2806	−174	−5
5	1693	1649		−44	1649	−44	0	1649	−44	0	1649	−44	0
6	1632	1569	(−15)	−62	1576	−56	7	1578	−53	9	1578	−53	9
7	1479	1443		−36	1443	−36	0	1443	−36	0	1443	−36	0
8	1402	1342		−60	1342	−60	0	1342	−60	0	1342	−60	0
9	1391	1334		−56	1334	−56	0	1334	−56	0	1334	−56	0
10	1287	1265	(1)	−22	1271	−17	5	1268	−20	2	1268	−20	2
11	1117	1102		−15	1102	−15	0	1102	−15	0	1102	−15	0
12	1041	1015		−26	1015	−26	0	1015	−26	0	1015	−26	0
13	1018	989		−29	989	−29	0	989	−29	0	989	−29	0
14	1005	992		−13	992	−13	0	992	−13	0	992	−13	0
15	945	921		−24	921	−24	0	921	−24	0	921	−24	0
16	894	881		−13	881	−13	0	881	−13	0	881	−13	0
17	785	763		−22	763	−22	0	762	−23	−1	762	−23	−1
18	522	521		−1	521	−1	0	521	−1	0	521	−1	0
19	404	393		−11	393	−11	0	393	−11	0	393	−11	0
20	292	288		−3	288	−3	0	288	−3	0	288	−3	0
21	278	258		−20	258	−20	0	258	−20	0	258	−20	0
MIN							−20			−5			−5
MAX							82			24			24
MAE							6			2			2
TS													
1	3237	3106	(0)	−131	3107	−130	0	3110	−127	3	3110	−127	3
2	3092	2919	(−19)	−172	2948	−143	29	2947	−144	28	2947	−145	28
3	3091	2903	(−31)	−188	2949	−143	45	2947	−144	44	2947	−145	43
4	1876	1842		−35	1842	−35	0	1842	−35	0	1842	−35	0
5	1635	1601		−34	1601	−34	0	1601	−34	0	1601	−34	0
6	1618	1630		11	1420	−198	−209	1624	6	−5	1624	6	−5
7	1503	1473		−30	1473	−30	0	1473	−30	0	1473	−30	0
8	1368	1340	(−6)	−28	1341	−27	1	1342	−26	2	1342	−26	2
9	1328	1308		−20	1308	−20	0	1308	−20	0	1308	−20	0
10	1304	1240		−64	1240	−64	0	1240	−64	0	1240	−64	0
11	1113	1095		−18	1095	−18	0	1095	−18	0	1095	−18	0
12	1060	1042		−18	1042	−18	0	1042	−18	0	1042	−18	0
13	1039	1016		−22	1016	−22	0	1016	−22	0	1016	−22	0
14	990	968		−22	968	−22	0	968	−22	0	968	−22	0
15	946	941		−5	941	−5	0	941	−5	0	941	−5	0
16	780	760		−20	760	−20	0	759	−21	−1	759	−21	−1
17	618	629		11	629	11	0	629	11	0	629	11	0
18	576	567		−8	567	−8	0	567	−8	0	567	−8	0
19	399	391		−8	391	−8	0	390	−8	0	390	−8	0
20	370	357		−13	357	−13	0	357	−13	0	357	−13	0
MIN <sup>b</sup>							−209			−5			−5
MAX <sup>b</sup>							45			44			43
MAE <sup>c</sup>							14			4			4

<sup>a</sup>For GVPT2, the difference between deperturbed and variational values for modes involved in Fermi resonances is reported in parentheses.  $\Delta_{\text{GVPT2}}$  refers to the difference in the anharmonic correction with respect to the GVPT2 model. <sup>b</sup>MIN and MAX stands for signed errors, largest positive (MAX) and largest negative (MIN). See text. <sup>c</sup>MAE stands for Mean Absolute Error. See text.

In conclusion, anharmonic perturbative computations including, when needed, HR corrections, show a significant improvement over their simple harmonic counterparts. Moreover, the HDCPT2 model leads to results as good as the ones obtained by the well established GVPT2 scheme.

The computations described above provide also specific heats and thermal corrections to internal energy and enthalpy. Without going into further details, those contributions are closely related to zero point energies and entropies, so that a corresponding accuracy can be expected.



**Table 6.** Vibrational Partition Functions for H<sub>2</sub>O at Different Temperatures, Computed with the GVPT2, DCPT2, and HDCPT2 Approaches Using the Force Field Generated at the B3LYP/aug-N07D and B2PLYP/ aug-cc-pVTZ Levels and Hybrid CCSD(T)/CBS//B3LYP/ aug-N07D Approach, Compared to Other Theoretical Results Including Accurate Estimates Based on Experimentally Derived Force Field

T (K)	298	1000	2400	4000
p <sup>a</sup>	10	3	1	1
B3LYP/ aug-N07D				
Harmonic	1.52	1.32	1.19	7.38
GVPT2	2.17	1.48	1.30	8.13
DCPT2	2.17	1.48	1.30	8.13
HDCPT2	2.17	1.48	1.30	8.13
Anh - Harm	0.65	0.16	0.11	0.75
Anh/Harm	1.43	1.12	1.09	1.10
B2PLYP/ aug-cc-pVTZ				
Harmonic	1.51	1.31	1.19	7.39
GVPT2	2.15	1.48	1.30	8.12
DCPT2	2.15	1.48	1.30	8.12
HDCPT2	2.15	1.48	1.30	8.13
Anh-Harm	0.64	0.16	0.11	0.74
Anh/Harm	1.42	1.12	1.09	1.10
hybrid CCSD(T)/CBS//B3LYP/ aug-N07D				
Harmonic	1.31	1.26	1.16	7.22
GVPT2	1.85	1.41	1.26	7.92
DCPT2	1.85	1.41	1.26	7.92
HDCPT2	1.85	1.41	1.26	7.92
Anh-Harm	0.54	0.15	0.10	0.70
Anh/Harm	1.41	1.12	1.09	1.10
experimental HMS force field <sup>b</sup>				
Harmonic	1.32 <sup>c</sup>	1.26 <sup>d</sup>	1.16 <sup>d</sup>	7.24 <sup>d</sup>
PT2	1.87 <sup>c</sup>	1.38 <sup>e</sup>	1.25 <sup>e</sup>	7.91 <sup>e</sup>
DCPT2	1.86 <sup>c</sup>			
RCPT2	1.87 <sup>c</sup>			
Accurate	1.76 <sup>c</sup>	1.39 <sup>d</sup>	1.26 <sup>d</sup>	8.06 <sup>d</sup>
Anh-Harm	0.44	0.13	0.10	0.82
Anh/Harm	1.33	1.10	1.09	1.11

<sup>a</sup>Power of 10 by which the values in this column have been multiplied. <sup>b</sup>The experimentally derived Hoy–Mills–Stray (HMS) quartic general force field.<sup>98</sup> <sup>c</sup>From ref 61. <sup>d</sup>From refs 57 and 58. <sup>e</sup>From ref 56.

In general, the total molar entropy of a species can be written as

$$S_g^\circ = \sum_{i=1}^n x_i S_i - R \sum_{i=1}^n x_i \ln x_i \quad (31)$$

where  $n$  is the number of different energy minima and  $x$  their respective molar fraction. The second term is known as the entropy of mixing. Thus, the procedure described above should be repeated for the different minima and combined with the percentages issuing from a Boltzmann distribution based on the computed energies of the minima. It is readily verified that  $R \ln(n)$ , the entropy of mixing of  $n$  equally populated minima, represents a reasonable approximation to  $\Delta S_{\text{mix}}$  provided that only low-energy conformers ( $\approx 4$  kJ mol<sup>-1</sup> above the absolute minimum) are counted. Furthermore, the entropies of nearly iso-energetic minima are usually very close and can be well approximated by the

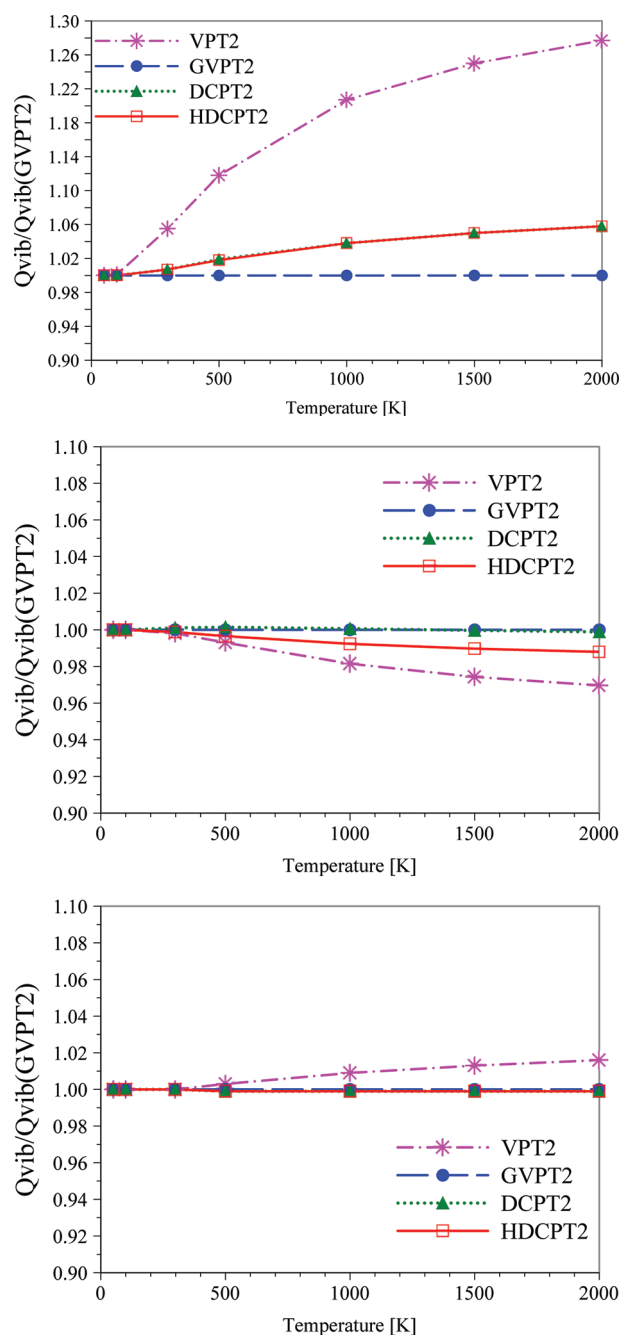


**Figure 2.** Anharmonic vibrational partition functions ( $Q_{\text{vib}}$ ) relative to GVPT2 for glycine (top), uracil (center), and pyrimidine (bottom) at different temperatures. GVPT2, VPT2, DCPT2, and HDCPT2 computations based on the force field generated at the B3LYP/ aug-N07D level. The hindered rotor model<sup>95–97</sup> has been applied to the two lowest frequency modes of glycine.

value computed for the absolute minimum ( $S_{\text{min}}^\circ$ ). As a consequence, eq 31 becomes

$$S_g^\circ = S_{\text{min}}^\circ + R \ln(n) \quad (32)$$

and multiple minima systems do not require additional computations with respect to their single-minimum counterparts, except for the definition of  $n$ , which can be correctly obtained at lower computational levels. The reliability of this approach at the harmonic level has been

**Table 7. Absolute Entropies ( $\text{J mol}^{-1} \text{K}^{-1}$ ) at 298.15 K and 1 atm Computed with the VPT2, GVPT2 and HDCPT2 Approaches Using the Force Field Generated at the B3LYP/aug-N07D Level Compared to Available Experimental Results<sup>a</sup>**

		harmonic	VPT2	GVPT2 no rotor	HDCPT2	exptl. <sup>b</sup>
H <sub>2</sub> O		188.72	188.72	188.72	188.72	188.72 <sup>c</sup>
H <sub>2</sub> S		205.78	205.80	205.80	205.80	205.65 <sup>c</sup>
H <sub>2</sub> CO		218.60	218.64	218.64	218.64	218.84 <sup>c</sup>
C <sub>2</sub> H <sub>4</sub>		218.99	219.14	219.14	219.14	219.22 <sup>c</sup>
formic acid		248.39	248.77	248.86	248.74	248.88 <sup>d</sup>
uracil		330.36	331.77	331.80	331.83	
pyridine		281.53	282.46	282.46	282.46	282.80 <sup>e</sup>
pyrimidine		286.22	286.99	286.97	286.96	
	HR			rotors		
CH <sub>3</sub> OH	corrected	240.05	239.59	239.59	239.60	239.70 <sup>d</sup>
	uncorrected	238.48	238.02	238.02	238.03	
CH <sub>3</sub> SH	corrected	255.86	255.35	255.39	255.39	255.06 <sup>d</sup>
	uncorrected	254.21	253.70	253.74	253.74	
CH <sub>3</sub> CHO	corrected	264.19	263.96	263.96	263.96	263.84 <sup>d</sup>
	uncorrected	262.32	262.09	262.09	262.09	
CHO-CHO	corrected	272.53	272.04	272.04	272.03	272.39 <sup>f</sup>
	uncorrected	271.86	271.37	271.37	271.36	
toluene	corrected	329.06	326.19	326.20	326.20	320.66 <sup>e</sup>
	uncorrected	337.93	335.06	335.07	335.07	

<sup>a</sup>Hindered rotor (HR) contributions were computed by mean of an automatic procedure.<sup>95–97</sup> <sup>b</sup>Experimental values have been lowered by 0.11  $\text{J mol}^{-1} \text{K}^{-1}$  from the original 1 bar = 0.1 MPa values to correspond to 1 atm = 0.101325 MPa values. <sup>c</sup>From ref 122. <sup>d</sup>From ref 123. <sup>e</sup>From ref 124. <sup>f</sup>From ref 125.

**Table 8. Thermodynamic Properties of the Two Lowest-Energy Conformers of Glycine<sup>a</sup>**

	glycine I				glycine II				
	Harm	SPT	HR	SPT+HR	Harm	SPT	HR	SPT+HR	total
$\Delta G$ [ $\text{kJ mol}^{-1}$ ]	223.6	220.9	0.2	221.1	224.2	221.4	0.1	221.5	221.2
$\Delta H$ [ $\text{kJ mol}^{-1}$ ]	226.0	223.4	3.0	226.4	226.7	223.9	3.4	227.3	223.6
$\Delta S$ [ $\text{J mol}^{-1} \text{K}^{-1}$ ]	314.5	314.7	9.3	324.0	310.1	310.6	11.1	321.7	324.4(1.3 <sup>b</sup> )
$C_p$ [ $\text{J mol}^{-1} \text{K}^{-1}$ ]	78.5	80.2	−2.0	78.3	75.6	77.7	−1.2	76.4	77.6

<sup>a</sup>All values at 298.15 K and 1 atm computed by the HDCPT2 model using the force field generated at the B3LYP/aug-N07D level compared to available experimental results. Hindered rotor contributions computed by automatic procedure.<sup>95–97</sup> <sup>b</sup>Entropy of mixing.

convincingly shown in several works,<sup>103–105</sup> and these results extend, of course, to our approach.

For purposes of illustration, we report in Table 8 the results obtained for glycine, which is characterized by the presence of the two nearly iso-energetic minima separated by a non-negligible energy barrier which is not related to any single internal rotation<sup>135</sup> (see Figure 1). However, each conformer is characterized by the presence of two large amplitude internal rotations (around N–C and C–C bonds). The enthalpy and free energy of the most stable isomer are very close to those of the second energy minimum, but this is not exactly the case for entropy and specific heat, which, moreover receive non-negligible contributions from hindered rotations. Entropy of mixing cannot be neglected (1.3  $\text{J mol}^{-1} \text{K}^{-1}$ ) but is well approximated by  $R \ln(2)$  (1.4  $\text{J mol}^{-1} \text{K}^{-1}$ ). The final total entropy (324.5  $\text{J mol}^{-1} \text{K}^{-1}$ ) is very close to that of the absolute minimum due to a fortunate compensation between the contribution of the second minimum and the entropy of mixing (−0.8 and 1.3  $\text{J mol}^{-1} \text{K}^{-1}$ , respectively). So in this case, use of just global energy minimum provides a slightly more reliable result than use of eq 32 (324.0 vs 325.4 to be compared with

324.5  $\text{J mol}^{-1} \text{K}^{-1}$ ). All results including hindered rotations are, anyway, within the expected error bars for this kind of computation.

**4.3. Vibrational Frequencies with the GVPT2, DCPT2, and HDCPT2 Approaches.** In order to validate perturbative approaches also for spectroscopic studies, a more detailed discussion about the accuracy of anharmonic vibrational frequencies computed by different models is required. We start by presenting harmonic and anharmonic frequencies for a few small closed- and open-shell molecules (H<sub>2</sub>O, NH<sub>3</sub>, HCO, NH<sub>2</sub>) computed using the GVPT2, DCPT2, and HDCPT2 approaches, which are then compared to the best theoretical estimates and experimental data in Table 9. This first set of molecules has been chosen since it does not cause problems for the standard VPT2 computations, which already provide reliable frequencies. In this respect, the results reported in Table 9 show that both DCPT2 and HDCPT2 models provide results as accurate as those coming from GVPT2 computations. Additionally, in line with what has been discussed for diatomic molecules, the anharmonic frequencies computed at the B3LYP/aug-N07D

Table 9. Harmonic and Anharmonic Frequencies for a Few Small Closed- And Open-Shell Molecules ( $\text{H}_2\text{O}$ ,  $\text{NH}_3$ ,  $\text{HCO}$ ,  $\text{NH}_2$ ) Computed Using GVPT2, DCPT2, and HDCPT2 Approaches and Compared to the Best Theoretical Estimates and Experimental Data<sup>a</sup>

molecule	mode	B3LYP/aug-N07D					B2PLYP/aug-cc-pVTZ					CCSD(T)			exptl <sup>b</sup>
		$\omega$	$\nu_{\text{GVPT2}}$	$\nu_{\text{DCPT2}}$	$\nu_{\text{HDCPT2}}$	$\Delta_{\text{anh}}$	$\omega$	$\nu_{\text{GVPT2}}$	$\nu_{\text{DCPT2}}$	$\nu_{\text{HDCPT2}}$	$\Delta_{\text{anh}}$	$\omega$	$\nu$	$\Delta_{\text{anh}}$	
$\text{H}_2\text{O}$	$\nu_1$	3810	3637	3637	3636	-174	3812	3641	3642	3642	-171	3836 <sup>c</sup>	3659 <sup>c</sup>	-177	3657
	$\nu_2$	1640	1585	1584	1584	-55	1635	1582	1581	1581	-53	1650 <sup>c</sup>	1596 <sup>c</sup>	-54	1595
	$\nu_3$	3920	3734	3735	3734	-186	3924	3740	3741	3740	-183	3946 <sup>c</sup>	3758 <sup>c</sup>	-188	3756
$\text{HCO}$	$\nu_1$	2662	2419	2418	2419	-243	2707	2467	2466	2466	-241	2717 <sup>d</sup>	2460 <sup>d</sup>	-257	2435
	$\nu_2$	1930	1906	1906	1906	-24	1886	1862	1862	1862	-24	1905 <sup>d</sup>	1878 <sup>d</sup>	-27	1868
	$\nu_3$	1101	1068	1067	1067	-34	1112	1080	1079	1079	-33	1120 <sup>d</sup>	1093 <sup>d</sup>	-27	1081
$\text{NH}_2$	$\nu_1$	3358	3204	3204	3204	-154	3392	3242	3242	3242	-150	3377 <sup>e</sup>	3219 <sup>e</sup>	-157	3219
	$\nu_2$	1538	1493	1492	1492	-46	1541	1495	1495	1495	-46	1549 <sup>e</sup>	1504 <sup>e</sup>	-44	1497
	$\nu_3$	3453	3284	3285	3284	-169	3487	3322	3323	3322	-165	3471 <sup>e</sup>	3297 <sup>e</sup>	-173	3301
$\text{NH}_3$	$\nu_1$	3469	3353(3323)*	3321	3320	-149	3488	3348	3344	3345	-143	3489 <sup>f</sup>	3342 <sup>g</sup>	-147	3336
	$\nu_2$	1073	996	996	996	-77	1037	954	953	953	-84	1076 <sup>f</sup>	934 <sup>g</sup>	-142	932
	$\nu_3$	3594	3421	3422	3422	-172	3617	3450	3449	3449	-168	3619 <sup>f</sup>	3449 <sup>g</sup>	-170	3444
MAE(CCSD(T)) <sup>h</sup>	$\nu_4$	1666	1631*	1618	1618	-48	1673	1626	1625	1626	-48	1680 <sup>f</sup>	1629 <sup>g</sup>	-51	1626
	MAE (Exp) <sup>i</sup>		23	24	24			13	13	13					
			20	20	21			13	13	13					6

<sup>a</sup>For perturbative computations, the force fields have been generated at the B3LYP/aug-N07D and B2PLYP/aug-cc-pVTZ levels of theory. For GVPT2 results, modes involved in Fermi resonances are marked by an asterisk, while the DVPT2 values are reported in parentheses. All values are in  $\text{cm}^{-1}$ . <sup>b</sup>Experimental results from references:  $\text{H}_2\text{O}$ ,<sup>126</sup>  $\text{HCO}$ ,<sup>127</sup>  $\text{NH}_3$ ,<sup>128,129</sup> and  $\text{NH}_2$ ,<sup>130-132</sup> Frequencies (both harmonic and anharmonic) from variational computations with CCSD(T)/CBS quality sixth-order polynomial surface, ref 133. <sup>c</sup>Harmonic frequencies computed at the CCSD(T)/CBS level and anharmonic perturbative corrections from CCSD(T)/cc-pVQZ computations, see ref 134. <sup>d</sup>Harmonic and perturbative anharmonic computations at the CCSD(T)/cc-pVQZ level, see ref 48. <sup>e</sup>Harmonic frequencies computed at the CCSD(T)/cc-pwCVQZ level, see ref 88. <sup>f</sup>Variational computations with an exact kinetic energy operator based on six-dimensional PES obtained from CCSD(T)/aug-cc-pVQC and CCSD(T)/aug-cc-pVTZ computations, with subsequent fitting of the  $V_0$  term to experimental values of  $^{14}\text{NH}_3$ , see ref 89. <sup>g</sup>MAE(CCSD(T)) stands for Mean Absolute Error with respect to results computed at the CCSD(T) level. <sup>h</sup>MAE(Exp) stands for Mean Absolute Error with respect to experimental results.

Table 10. Anharmonic Frequencies (in  $\text{cm}^{-1}$ ) for for GLY Ip ( $C_s$ ) Conformer of Glycine Computed with the GVPT2, VPT2, DCPT2, and HDCPT2 Approaches Using the Force Field Generated at the B3LYP/aug-N07D Level and Compared to Experimental Data<sup>a</sup>

mode	sym.	GVPT2			VPT2			DCPT2			HDCPT2			assignment <sup>c</sup>
		$\omega$	$\nu$	$\Delta_{\text{anh}}$	$\nu$	$\Delta_{\text{anh}}$	$\Delta_{\text{GVPT2}}$	$\nu$	$\Delta_{\text{anh}}$	$\Delta_{\text{GVPT2}}$	$\nu$	$\Delta_{\text{anh}}$	$\Delta_{\text{GVPT2}}$	
1	A'	3750	3568	-182	3568	-182	0	3565	-185	-3	3566	-184	-2	OH stretch
3	A'	3509	3387	-122	3353	-156	-34	3304	-205	-83	3350	-159	-37	NH <sub>2</sub> (S) stretch
5	A'	3044	2938	-106	2913	-131	-25	2911	-133	-27	2910	-134	-28	CH <sub>2</sub> (S) stretch
6	A'	1816	1784	(32)	1784	-32	0	1784	-32	0	1784	-32	0	C=O stretch
7	A'	1673	1627	-46	1614	-59	-13	1614	-59	-13	1614	-59	-13	NH <sub>2</sub> bend
8	A'	1453	1431	(-22)	1417	-36	-14	1416	-37	-15	1416	-37	-15	CH <sub>2</sub> bend x
9	A'	1396	1354	(3)	1414	18	60	1375	-21	21	1375	-21	21	CH <sub>2</sub> bend z
11	A'	1305	1290	(-25)	1454	149	164	1289	-16	-1	1289	-16	-1	(OH+CH <sub>2</sub> x) bend
13	A'	1166	1123	(8)	1125	-41	2	1126	-40	3	1126	-40	3	CN str. + OH bend
14	A'	1129	1097	-32	1097	-32	0	1097	-32	0	1097	-32	0	CO str. + OH bend
15	A'	921	870	-51	868	-53	-2	870	-51	0	869	-52	-1	CC str. + NH <sub>2</sub> bend
17	A'	821	807	-14	799	-22	-8	798	-23	-9	798	-23	-9	CC stretch
19	A'	634	630	-4	630	-4	0	630	-4	0	630	-4	0	(NH <sub>2</sub> + OCO) bend
21	A'	464	461	-3	460	-4	-1	460	-4	-1	460	-4	-1	
22	A'	257	261	(1)	258	1	-3	258	1	-3	258	1	-3	
2	A''	3582	3407	-175	3407	-175	0	3404	-178	-3	3403	-179	-4	NH <sub>2</sub> (A) stretch
4	A''	3079	2929	-150	2926	-153	-3	2926	-153	-3	2925	-154	-4	CH <sub>2</sub> (A) stretch
10	A''	1382	1344	(1)	1347	-35	3	1346	-36	2	1346	-36	2	CH <sub>2</sub> NH <sub>2</sub> twist
12	A''	1181	1155	(0)	1155	-26	0	1155	-26	0	1155	-26	0	CH <sub>2</sub> NH <sub>2</sub> twist
16	A''	914	909	-5	909	-5	0	909	-5	0	909	-5	0	CH <sub>2</sub> NH <sub>2</sub> twist
18	A''	649	626	-23	626	-23	0	604	-45	-22	605	-44	-21	OH oop bend
20	A''	507	497	-10	497	-10	0	497	-10	0	497	-10	0	OH oop bend
23	A''	210	230	20	230	20	0	231	21	1	230	20	0	
24	A''	65	95	30	95	30	0	100	35	5	95	30	0	
	MIN <sup>e</sup>	-20			-45		-34	-47		-83	-48		-37	
	MAX <sup>e</sup>	7			41		164	5		21	5		21	
	MAE <sup>f</sup>	8			13		16	11		10	11		8	

<sup>a</sup>For GVPT2, the difference between deperturbed and variational values for modes involved in Fermi resonances is reported in parentheses.  $\Delta_{\text{GVPT2}}$  refers to the difference in the anharmonic correction with respect to the GVPT2 model. The relative errors with respect to experimental data are shown in bold. <sup>b</sup>Ref 106. <sup>c</sup>(A) and (S) refer to "asymmetric" and "symmetric" respectively; oop stands for out-of-plane. <sup>d</sup>Absolute errors relative to mode 1 have been calculated with respect to experimental data of ref 115. <sup>e</sup>MIN and MAX stands for signed errors, largest positive (MAX) and largest negative (MIN). See text. <sup>f</sup>MAE stands for Mean Absolute Error. See text.



Table 11. Anharmonic Frequencies (in  $\text{cm}^{-1}$ ) for Uracil Computed by GVPT2, VPT2, DCPT2, and HDCPT2 Approaches Using the Force Field Generated at the B3LYP/aug-N07D Level and Compared to Experimental Data<sup>a</sup>

mode	sym.	$\omega$	GVPT2		VPT2			DCPT2			HDCPT2			exptl. <sup>b</sup>	assignment <sup>c</sup>
			$\nu$	$\Delta_{\text{anh}}$	$\nu$	$\Delta_{\text{anh}}$	$\Delta_{\text{GVPT2}}$	$\nu$	$\Delta_{\text{anh}}$	$\Delta_{\text{GVPT2}}$	$\nu$	$\Delta_{\text{anh}}$	$\Delta_{\text{GVPT2}}$		
1	A'	3641	3472	−169	3381	−260	−91	3467	−174	−5	3472	−169	0	3485	$\nu(\text{N1-H})$
2	A'	3596	3430	−166	3362	−235	−68	3425	−171	−5	3429	−168	−1	3435	$\nu(\text{N3-H})$
3	A'	3249	3113	−136	3099	−150	−14	3113	−136	0	3113	−136	0		$\nu(\text{C5-H})$
4	A'	3208	3063	(12)	3078	−129	16	3083	−125	21	3083	−125	21		$\nu(\text{C6-H})$
5	A'	1799.0	1771	(−2)	1776	−23	6	1772	−27	1	1772	−27	1	1764	$\nu(\text{C2=O})$
6	A'	1764.0	1748	(−8)	1753	−11	5	1741	−24	−7	1741	−24	−7	1706	$\nu(\text{C4=O})$
7	A'	1674.0	1640		1647	−27	7	1640	−34	0	1640	−34	0	1643	$\nu(\text{C5=C6})$
8	A'	1500.0	1455	(4)	1475	−25	20	1465	−35	10	1465	−35	10	1472	$\delta(\text{N1-H})$
9	A'	1404.0	1367	(3)	1361	−43	−6	1367	−36	0	1367	−36	0	1400	$\delta(\text{C6-H})$
10	A'	1418.0	1390	(−4)	1388	−30	−2	1389	−29	−1	1389	−29	−1	1389	$\delta(\text{N3-H})$
11	A'	1383.0	1349	(0)	1346	−37	−2	1350	−33	1	1350	−33	1	1359	$\delta(\text{C5-H})$
12	A'	1229.0	1205	(−3)	1204	−25	0	1204	−25	0	1204	−25	0	1217	$\nu(\text{ring})$
13	A'	1196.0	1167		1167	−29	0	1167	−29	0	1167	−29	0	1185	$\nu(\text{ring})$
14	A'	1087.0	1064	(2)	1066	−20	2	1067	−20	3	1067	−20	3	1075	$\nu(\text{ring})$
15	A'	993.0	979	(−1)	995	3	17	980	−13	2	980	−13	2	980	$\nu(\text{ring})$
16	A'	973.0	946		928	−45	−18	946	−28	0	946	−28	0	958	$\nu(\text{ring})$
17	A'	771.0	753		759	−12	6	754	−17	1	754	−17	1	759	$\nu(\text{ring})$
18	A'	558.0	557		478	−79	−79	554	−4	−3	558	1	2	562	$\delta(\text{ring})$
19	A'	542.0	534		530	−12	−4	534	−9	−1	534	−9	−1	537	$\delta(\text{ring})$
20	A'	521.0	515		515	−6	0	515	−6	0	515	−6	0	516	$\delta(\text{ring})$
21	A'	387.0	387		384	−3	−3	387	0	0	387	0	0	391	$\delta(\text{C=O})$
22	A''	965.0	947		949	−17	2	946	−19	0	946	−19	0	987	$\gamma(\text{C6-H})$
23	A''	824.0	804		796	−27	−8	804	−20	0	804	−20	0	804	$\gamma(\text{C5-H})$
24	A''	767.0	747		749	−18	2	747	−20	0	747	−20	0	757	$\gamma(\text{C2=O})$
25	A''	731.0	715		709	−21	−5	715	−16	0	715	−16	0	718	$\gamma(\text{C4=O})$
26	A''	676.0	658	(1)	601	−75	−58	658	−18	−1	661	−15	2	662	$\gamma(\text{N3-H})$
27	A''	559.0	549	(4)	548	−11	−2	550	−10	0	550	−10	0	551	$\gamma(\text{N1-H})$
28	A''	399.0	394		394	−5	0	395	−5	1	395	−5	1	411	$\gamma(\text{ring})$
29	A''	169.0	165		162	−6	−3	165	−4	0	165	−4	0	185	$\gamma(\text{ring})$
30	A''	154.0	147		143	−11	−4	147	−7	0	147	−7	0		$\gamma(\text{ring})$
MIN <sup>d</sup>			−40		−104		−91	−41		−7	−41		−7		
MAX <sup>d</sup>			42		47		20	35		21	35		21		
MAE <sup>e</sup>			11		24		15	11		2	10		2		

<sup>a</sup>For GVPT2, the difference between deperturbed and variational values for modes involved in Fermi resonances is reported in parentheses.  $\Delta_{\text{GVPT2}}$  refers to the difference in the anharmonic correction with respect to the GVPT2 model. The relative errors with respect to experimental data are shown in bold. <sup>b</sup>Refs 107–109. <sup>c</sup>Assignment checked through visual inspection of atomic displacements along normal modes;  $\nu$ ,  $\delta$ , and  $\gamma$  refer to stretching, bending, and deformation vibrations, respectively. <sup>d</sup>MIN and MAX stands for signed errors, largest positive (MAX) and largest negative (MIN). See text. <sup>e</sup>MAE stands for Mean Absolute Error. See text.

level already agree quite well with the best available theoretical and experimental data, while further improvements are obtained by B2PLYP/aug-cc-pVTZ computations. Moreover, it is shown that anharmonic corrections provided by both DFT models agree very well with their highly accurate counterparts, often computed using sophisticated theoretical models combined with highly accurate electronic structure computations. The only significant discrepancy is observed for the  $\nu_2$  mode of ammonia, and for this mode the DFT computations lead to a better agreement with experimental results than the hybrid CC/DFT approach. The case of  $\text{NH}_3$  shows additionally that the automatic procedure to identify resonance interactions leads to different results with two electronic structure models, a  $\nu_1-2\nu_4$  resonance being detected for B3LYP computations, while no Fermi interaction has been identified when B2PLYP functional has been applied to compute harmonic frequencies and force constants. Although such a discrepancy did not cause problems and both computations yield accurate results, this could not be the case for larger systems.

As a final validation, the GVPT2, VPT2, DCPT2, and HDCPT2 approaches (in conjunction with force fields generated at the B3LYP/aug-N07D level) have been compared for the anharmonic frequencies of glycine, uracil, and pyrimidine. These medium-size molecules have been chosen on the basis of the accuracy of GVPT2 computations with respect to well-established experimental data.<sup>106–110</sup> The results gathered in Tables 10–12 clearly show the advantages of the HDCPT2 model introduced in this work, which always delivers anharmonic frequencies of an accuracy close to that of the GVPT2 model, but through a completely “threshold-free” and general procedure. It should be highlighted that the improved accuracy over DCPT2 is evident in the case of glycine (the maximum discrepancy with respect to GVPT2 decreases by about  $50 \text{ cm}^{-1}$ ), where strong couplings between low- and high-frequency vibrations within the  $\text{NH}_2$  group are observed. It is also worth noting that HDCPT2 computations provided very accurate results even in such a difficult case as uracil, whose spectrum is plagued by several Fermi resonances.

Table 12. Anharmonic Frequencies (in  $\text{cm}^{-1}$ ) for Pyrimidine Computed by GVPT2, VPT2, DCPT2, and HDCPT2 Approaches Using the Force Field Generated at the B3LYP/aug-N07D Level and Compared to Experimental Data<sup>a</sup>

mode <sup>b</sup>	sym.	$\omega$	GVPT2			VPT2			DCPT2			HDCPT2			exptl. <sup>c</sup>	assignment <sup>d</sup>
			$\nu$	$\Delta_{\text{anh}}$		$\nu$	$\Delta_{\text{anh}}$	$\Delta_{\text{GVPT2}}$	$\nu$	$\Delta_{\text{anh}}$	$\Delta_{\text{GVPT2}}$	$\nu$	$\Delta_{\text{anh}}$	$\Delta_{\text{GVPT2}}$		
1	A1	3203	3055(7)	−148		3062	−141	7	3067	−136	12	3067	−136	12	3091	$\nu_{\text{C3H3}}$
2	A1	3175	3053(−16)	−122		3049	−126	−4	3047	−128	−6	3047	−128	−6	3057	$\nu_{\text{C1H1}}$
3	A1	3158	3030	−128		3030	−128	0	3030	−128	0	3029	−129	−1	3041	$\nu_{\text{CHsym}}$
4	A1	1616	1573	−43		1573	−43	0	1573	−43	1	1573	−43	1	1567	$\nu_{\text{CCsym}} + \nu_{\text{CNsym}}$
5	A1	1437	1408	−29		1408	−29	0	1408	−29	0	1408	−29	0	1401	$\delta_{\text{CHsym}} + \nu_{\text{CNsym}}$
6	A1	1161	1141	−20		1141	−20	0	1141	−20	0	1141	−20	0	1138	$\nu_{\text{CNsym}} + \delta$ ring
7	A1	1079	1053(9)	−26		1052	−27	−1	1056	−23	3	1056	−23	3	1071	$\nu_{\text{CCsym}} + \delta$ ring
8	A1	1013	997	−16		997	−16	0	997	−16	0	997	−16	0	990	$\delta$ ring + $\nu_{\text{CNsym}}$
9	A1	692	683	−9		683	−9	0	683	−9	0	683	−9	0	678	$\delta$ ring
12	B2	3162	3033	−129		3033	−129	0	3032	−130	0	3032	−130	−1	3052	$\nu_{\text{CHas}}$
13	B2	1616	1557	−59		1571	−45	14	1574	−42	17	1574	−42	17	1571	$\nu_{\text{CCas}} + \nu_{\text{CNas}}$
14	B2	1495	1463	−32		1463	−32	0	1463	−32	0	1463	−32	0	1465	$\delta_{\text{CH}}$
15	B2	1390	1362(−1)	−28		1363	−27	1	1362	−28	0	1362	−28	0	1374	$\delta_{\text{CH}}$
16	B2	1262	1228	−34		1228	−34	0	1228	−34	0	1228	−34	0	1223	$\nu_{\text{CN}} + \delta_{\text{CH}}$
17	B2	1228	1197(4)	−31		1170	−58	−27	1195	−33	−2	1195	−33	−2	1157	$\nu_{\text{CNas}} + \nu_{\text{CCas}}$
18	B2	1095	1075	−20		1075	−20	0	1075	−20	0	1075	−20	0	1074	$\delta_{\text{CH}}$
19	B2	634	626	−8		626	−8	0	626	−8	0	626	−8	0	621	$\delta$ ring
20	B1	1022	1002	−20		1002	−20	0	1002	−20	0	1002	−20	0		$\gamma_{\text{CHsym}}$
21	B1	980	958	−22		958	−22	0	958	−22	0	958	−22	0		$\gamma_{\text{CH}}$
22	B1	821	807	−14		807	−14	0	807	−14	0	807	−14	0	803	$\tau$ ring + $\gamma_{\text{CH}}$
23	B1	738	723	−15		723	−15	0	723	−15	0	723	−15	0	719	$\tau$ ring + $\gamma_{\text{CH}}$
24	B1	351	344	−7		344	−7	0	344	−7	0	344	−7	0		$\tau$ ring
10	A2	998	979	−19		979	−19	0	979	−19	0	979	−19	0		$\gamma_{\text{CHas}}$
11	A2	408	400	−8		400	−8	0	400	−8	0	400	−8	0		$\tau$ ring
	MIN <sup>e</sup>		−36			−29		−27	−25		−6	−25		−6		
	MAX <sup>e</sup>		40			13		14	38		17	38		17		
	MAE <sup>f</sup>		11			8		2	10		2	10		2		

<sup>a</sup>For GVPT2, the difference between deperturbed and variational values for modes involved in Fermi resonances is reported in parentheses.  $\Delta_{\text{GVPT2}}$  refers to the difference in the anharmonic correction with respect to the GVPT2 model. The relative errors with respect to experimental data are shown in bold. <sup>b</sup>Normal mode numbering as in refs 43, 46, and 110. <sup>c</sup>The most recent experimental data (FTIR spectrum of pyrimidine isolated in solid argon form ref 110). <sup>d</sup>Assignment from ref 110 based on the Potential Energy Distribution (PED) analysis, checked through visual inspection of atomic displacements along normal modes.  $\nu$ ,  $\delta$ ,  $\gamma$ , and  $\tau$  refer to stretching, bending, and deformation vibrations, respectively. <sup>e</sup>MIN and MAX stands for signed errors, largest positive (MAX) and largest negative (MIN). See text. <sup>f</sup>MAE stands for Mean Absolute Error. See text.

## CONCLUSIONS

A general perturbative model allowing computation of spectroscopic, thermodynamic, and kinetic properties for medium-to-large semirigid molecular systems in a fully automated manner has been presented. Its basic ingredients are zero-point energies obtained according to a singularity-free equation, anharmonic vibrational computations by means of the hybrid degeneracy-corrected second-order vibrational perturbation theory, and partition functions obtained from the simple perturbation theory extended to treat both energy minima and transition states. The necessary validations have been performed for a large benchmark of small-to-medium-size, closed- and open-shell, molecular systems. In particular, zero-point vibrational energies, vibrational partition functions, entropies, and vibrational frequencies have been considered, showing in all cases good agreement with available accurate experimental and theoretical data. Additionally, the reliability of the results from DFT computations has been assessed through the comparison with their accurate experimental and theoretical counterparts, showing also that possible discrepancies should be mostly attributed to the harmonic component. These

findings are of relevance for the definition of hybrid models, which pave the route toward the accurate computation of spectroscopic and thermochemical properties for molecules with larger and larger numbers of atoms.

Furthermore, the general model introduced in the present work allows reliable computations of spectroscopic and thermochemical properties also for difficult cases with several Fermi resonances (uracil) or with strong couplings between low- and high-frequency modes (glycine, toluene). It should be also stressed that this approach, implemented in the Gaussian suite, can be applied in conjunction with any quantum mechanical model for which analytical Hessians are available. This means that, together with isolated molecules, a black-box procedure to evaluate spectroscopic and thermochemical properties beyond the harmonic approximation is available also for systems in solution described by the polarizable continuum model. Additionally, properly tailored reduced-dimension anharmonic approaches allow one to take into account simultaneously anharmonic and environmental effects on the vibrational properties even for relatively large molecular systems. In conclusion, we strongly recommend use of the approach described in this work, in particular in conjunction with B3LYP/aug-N07D electronic structure computations or hybrid models, as a

fully general method to evaluate accurate anharmonic spectroscopic and thermochemical properties for medium-to-large semirigid molecular systems in the gas phase and in solution. Regarding a fully ab initio simulation of vibrational spectra, a general model set within vibrational perturbation theory, allowing computations of different band intensities (IR, VCD, etc.) in the gas phase and in solutions, has been recently introduced.<sup>32,68,111</sup> However, in this case, a proper treatment of resonances is less straightforward, and further developments along these lines are currently in progress in our laboratory.

## AUTHOR INFORMATION

### Corresponding Author

\*E-mail: julien.bloino@sns.it, vincenzo.barone@sns.it.

### Notes

The authors declare no competing financial interest.

## ACKNOWLEDGMENTS

This work was supported by Italian MIUR. The large scale computer facilities of the VILLAGE network (<http://m3village.sns.it>) are acknowledged for providing computer resources. The COST-CMTS Action CM1002 "CONvergent Distributed Environment for Computational Spectroscopy (CODECS)" is also acknowledged.

## REFERENCES

- (1) Barone, V. *Computational Strategies for Spectroscopy, from Small Molecules to Nano Systems*; John Wiley & Sons, Inc.: Hoboken, NJ, 2011.
- (2) Jensen, P.; Bunker, P. R. *Computational Molecular Spectroscopy*; John Wiley & Sons: New York, 2000.
- (3) Csaszar, A. G.; Fabri, C.; Szidarovszky, T.; Matyus, E.; Furtenbacher, T.; Czako, G. The fourth age of quantum chemistry: molecules in motion. *Phys. Chem. Chem. Phys.* **2012**, *14*, 1085–1106.
- (4) Cappelli, C.; Biczysko, M. In *Computational Strategies for Spectroscopy*; Barone, V., Ed.; John Wiley & Sons, Inc.: New York, 2011; pp 309–360.
- (5) Yang, X.; Liu, K. *Modern Trends in Chemical Reaction Dynamics: Experiment and Theory (Part 1)*, *Advanced Series in Physical Chemistry*; World Scientific: River Edge, NJ, 2004; Vol. 14.
- (6) Curtiss, L. A.; Raghavachari, K.; Trucks, G. W.; Pople, J. A. Gaussian-2 theory of molecular energies of first- and second-row compounds. *J. Chem. Phys.* **1991**, *94*, 7221–7230.
- (7) Irikura, K. K.; Johnson, I. R. D.; Kacker, R. N.; Kessel, R. Uncertainties in scaling factors for ab initio vibrational zero-point energies. *J. Chem. Phys.* **2009**, *130*, 114102.
- (8) Teixeira, F.; Melo, A.; Cordeiro, M. N. D. S. Calibration sets and the accuracy of vibrational scaling factors: A case study with the X3LYP hybrid functional. *J. Chem. Phys.* **2010**, *133*, 114109.
- (9) Pernot, P.; Cailliez, F. Comment on Uncertainties in scaling factors for ab initio vibrational zero-point energies [ *J. Chem. Phys.* **130**, 114102 (2009) ] and Calibration sets and the accuracy of vibrational scaling factors: A case study with the X3LYP hybrid functional [ *J. Chem. Phys.* **2010**, *133*, 114109 ]. *J. Chem. Phys.* **2011**, *134*, 167101.
- (10) Karton, A.; Rabinovich, E.; Martin, J. M. L.; Ruscic, B. W4 theory for computational thermochemistry: In pursuit of confident sub-kJ/mol predictions. *J. Chem. Phys.* **2006**, *125*, 144108.
- (11) Karton, A.; Taylor, P. R.; Martin, J. M. L. Basis set convergence of post-CCSD contributions to molecular atomization energies. *J. Chem. Phys.* **2007**, *127*, 064104.
- (12) Karton, A.; Daon, S.; Martin, J. M. W4–11: A high-confidence benchmark dataset for computational thermochemistry derived from first-principles W4 data. *Chem. Phys. Lett.* **2011**, *510*, 165–178.
- (13) Tajti, A.; Szalay, P. G.; Csaszar, A. G.; Kallay, M.; Gauss, J.; Valeev, E. F.; Flowers, B. A.; Vázquez, J.; Stanton, J. F. HEAT: High accuracy extrapolated ab initio thermochemistry. *J. Chem. Phys.* **2004**, *121*, 11599–11613.
- (14) Bomble, Y. J.; Vázquez, J.; Kallay, M.; Michauk, C.; Szalay, P. G.; Csaszar, A. G.; Gauss, J.; Stanton, J. F. High-accuracy extrapolated ab initio thermochemistry. II. Minor improvements to the protocol and a vital simplification. *J. Chem. Phys.* **2006**, *125*, 064108.
- (15) Harding, M. E.; Vázquez, J.; Ruscic, B.; Wilson, A. K.; Gauss, J.; Stanton, J. F. High-accuracy extrapolated ab initio thermochemistry. III. Additional improvements and overview. *J. Chem. Phys.* **2008**, *128*, 114111.
- (16) Curtiss, L. A.; Redfern, P. C.; Raghavachari, K. Gaussian-4 theory. *J. Chem. Phys.* **2007**, *126*, 084108.
- (17) Curtiss, L. A.; Redfern, P. C.; Raghavachari, K. Gaussian-4 theory using reduced order perturbation theory. *J. Chem. Phys.* **2007**, *127*, 124105.
- (18) Karton, A.; Gruzman, D.; Martin, J. M. L. Benchmark Thermochemistry of the  $C_nH_{2n+2}$  Alkane Isomers ( $n = 2-8$ ) and Performance of DFT and Composite Ab Initio Methods for Dispersion-Driven Isomeric Equilibria. *J. Phys. Chem. A* **2009**, *113*, 8434–8447.
- (19) Karton, A.; Ruscic, B.; Martin, J. M. Benchmark atomization energy of ethane: Importance of accurate zero-point vibrational energies and diagonal Born-Oppenheimer corrections for a 'simple' organic molecule. *THEOCHEM* **2007**, *811*, 345–353.
- (20) Mills, I. M. In *Molecular Spectroscopy: Modern Research*; Rao, K. N.; Mathews, C. W., Eds.; Academic: New York, 1972.
- (21) Amos, R. D.; Handy, N. C.; Green, W. H.; Jayatilaka, D.; Willets, A.; Palmieri, P. Anharmonic vibrational properties of  $CH_2F_2$ : A comparison of theory and experiment. *J. Chem. Phys.* **1991**, *95*, 8323.
- (22) Gaw, F.; Willets, A.; Handy, N.; Green, W. SPECTRO - a program for derivation of spectroscopic constants from provided quartic force fields and cubic dipole fields. *Advances in Molecular Vibrations and Collision Dynamics*; Bowman, J. M., Ed.; JAI Press Inc.: Greenwich, CT, 1991; Vol. 1B, pp 169–185.
- (23) Barone, V. Anharmonic vibrational properties by a fully automated second-order perturbative approach. *J. Chem. Phys.* **2005**, *122*, 014108.
- (24) Barone, V. Vibrational zero-point energies and thermodynamic functions beyond the harmonic approximation. *J. Chem. Phys.* **2004**, *120*, 3059–3065.
- (25) Martin, J. M. L.; Lee, T. J.; Taylor, P. M.; François, J.-P. The anharmonic force field of ethylene,  $C_2H_4$ , by means of accurate ab initio calculations. *J. Chem. Phys.* **1995**, *103*, 2589–2602.
- (26) Stanton, J. F.; Gauss, J. Anharmonicity in the ring stretching modes of diborane. *J. Chem. Phys.* **1998**, *108*, 9218–9220.
- (27) Ruud, K.; Taylor, P. R.; Helgaker, T. Automated calculation of fundamental frequencies: Application to  $AlH_3$  using the coupled-cluster singles-and-doubles with perturbative triples method. *J. Chem. Phys.* **2003**, *119*, 1951–1960.
- (28) Ruud, K.; Åstrand, P. O.; Taylor, P. R. An efficient approach for calculating vibrational wave functions and zero-point vibrational corrections to molecular properties of polyatomic molecules. *J. Chem. Phys.* **2000**, *112*, 2668–2683.
- (29) Vázquez, J.; Stanton, J. F. Simple(r) algebraic equation for transition moments of fundamental transitions in vibrational second-order perturbation theory. *Mol. Phys.* **2006**, *104*, 377–388.
- (30) Vázquez, J.; Stanton, J. F. Treatment of Fermi resonance effects on transition moments in vibrational perturbation theory. *Mol. Phys.* **2007**, *105*, 101–109.
- (31) Stanton, J. F.; Gauss, J. Analytic second derivatives in high-order many-body perturbation and coupled-cluster theories: Computational considerations and applications. *Int. Rev. Phys. Chem.* **2000**, *19*, 61–95.
- (32) Barone, V.; Bloino, J.; Guido, C. A.; Lipparini, F. A fully automated implementation of VPT2 Infrared intensities. *Chem. Phys. Lett.* **2010**, *496*, 157–161.
- (33) Bowman, J. M. Beyond Platonic Molecules. *Science* **2000**, *290*, 724–725.



- (34) Bowman, J. M.; Carter, S.; Huang, X. MULTIMODE: A code to calculate rovibrational energies of polyatomic molecules. *Int. Rev. Phys. Chem.* **2003**, *22*, 533–549.
- (35) Carter, S.; Handy, N. The vibrations of  $\text{H}_2\text{O}_2$ , studied by “multimode”, with a large amplitude motion. *J. Chem. Phys.* **2000**, *113*, 987–993.
- (36) Chaban, G.; Jung, J.; Gerber, R. Ab initio calculation of anharmonic vibrational states of polyatomic systems: Electronic structure combined with vibrational self-consistent field. *J. Chem. Phys.* **1999**, *111*, 1823–1829.
- (37) Rauhut, G.; Hrenar, T. A combined variational and perturbational study on the vibrational spectrum of  $\text{P}_2\text{F}_4$ . *Chem. Phys.* **2008**, *346*, 160–166.
- (38) Christiansen, O. Vibrational structure theory: new vibrational wave function methods for calculation of anharmonic vibrational energies and vibrational contributions to molecular properties. *Phys. Chem. Chem. Phys.* **2007**, *9*, 2942–2953.
- (39) Norris, L. S.; Ratner, M. A.; Roitberg, A. E.; Gerber, R. B. Moller-Plesset perturbation theory applied to vibrational problems. *J. Chem. Phys.* **1996**, *105*, 11261–11267.
- (40) Christiansen, O. Moller-Plesset perturbation theory for vibrational wave functions. *J. Chem. Phys.* **2003**, *119*, 5773–5781.
- (41) Carter, S.; Sharma, A. R.; Bowman, J. M.; Rosmus, P.; Tarroni, R. Calculations of rovibrational energies and dipole transition intensities for polyatomic molecules using MULTIMODE. *J. Chem. Phys.* **2009**, *131*, 224106.
- (42) Carbonniere, P.; Lucca, T.; Pouchan, C.; Rega, N.; Barone, V. Vibrational computations beyond the harmonic approximation: performances of the B3LYP functional for semirigid molecules. *J. Comput. Chem.* **2005**, *26*, 384–388.
- (43) Boese, A. D.; Martin, J. Vibrational Spectra of the Azabenzenes Revisited: Anharmonic Force Fields. *J. Phys. Chem. A* **2004**, *108*, 3085–3096.
- (44) Barone, V. Vibrational spectra of large molecules by density functional computations beyond the harmonic approximation: the case of pyrrole and furan. *Chem. Phys. Lett.* **2004**, *383*, 528–532.
- (45) Barone, V. Characterization of the potential energy surface of the  $\text{HO}_2$  molecular system by a density functional approach. *J. Chem. Phys.* **1994**, *101*, 10666–10676.
- (46) Barone, V. Accurate Vibrational Spectra of Large Molecules by Density Functional Computations beyond the Harmonic Approximation: The Case of Azabenzenes. *J. Phys. Chem. A* **2004**, *108*, 4146–4150.
- (47) Barone, V.; Bloino, J.; Biczysko, M. Validation of the DFT/N07D computational model on the magnetic, vibrational and electronic properties of vinyl radical. *Phys. Chem. Chem. Phys.* **2010**, *12*, 1092–1101.
- (48) Puzzarini, C.; Biczysko, M.; Barone, V. Accurate Harmonic/Anharmonic Vibrational Frequencies for Open-Shell Systems: Performances of the B3LYP/N07D Model for Semirigid Free Radicals Benchmarked by CCSD(T) Computations. *J. Chem. Theory Comput.* **2010**, *6*, 828–838.
- (49) Neese, F.; Schwabe, T.; Grimme, S. Analytic derivatives for perturbatively corrected “double hybrid” density functionals: Theory, implementation, and applications. *J. Chem. Phys.* **2007**, *126*, 124115.
- (50) Biczysko, M.; Panek, P.; Scalmani, G.; Bloino, J.; Barone, V. Harmonic and Anharmonic Vibrational Frequency Calculations with the Double-Hybrid B2PLYP Method: Analytic Second Derivatives and Benchmark Studies. *J. Chem. Theory Comput.* **2010**, *6*, 2115–2125.
- (51) Kozuch, S.; Gruzman, D.; Martin, J. M. L. DSD-BLYP: A General Purpose Double Hybrid Density Functional Including Spin Component Scaling and Dispersion Correction. *J. Phys. Chem. C* **2010**, *114*, 20801.
- (52) Puzzarini, C.; Barone, V. Toward spectroscopic accuracy for organic free radicals: Molecular structure, vibrational spectrum, and magnetic properties of  $\text{F}_2\text{NO}$ . *J. Chem. Phys.* **2008**, *129*, 084306/1–7.
- (53) Puzzarini, C.; Barone, V. Assessment of a computational strategy approaching spectroscopic accuracy for structure, magnetic properties and vibrational frequencies of organic free radicals: the  $\text{F}_2\text{CN}$  and  $\text{F}_2\text{BO}$  case. *Phys. Chem. Chem. Phys.* **2008**, *10*, 6991–6997.
- (54) Begue, D.; Carbonniere, P.; Pouchan, C. Calculations of Vibrational Energy Levels by Using a Hybrid ab Initio and DFT Quartic Force Field: Application to Acetonitrile. *J. Phys. Chem. A* **2005**, *109*, 4611–4616.
- (55) Begue, D.; Benidar, A.; Pouchan, C. The vibrational spectra of vinylphosphine revisited: Infrared and theoretical studies from CCSD(T) and DFT anharmonic potential. *Chem. Phys. Lett.* **2006**, *430*, 215–220.
- (56) Truhlar, D. G.; Isaacson, A. D. Simple perturbation theory estimates of equilibrium constants from force fields. *J. Chem. Phys.* **1991**, *94*, 357–359.
- (57) Isaacson, A. D.; Truhlar, D. G.; Scanlon, K.; Overend, J. Tests of approximation schemes for vibrational energy levels and partition functions for triatomics:  $\text{H}_2\text{O}$  and  $\text{SO}_2$ . *J. Chem. Phys.* **1981**, *75*, 3017–3024.
- (58) Isaacson, A. D.; Zhang, X.-G. Vibrational partition functions for  $\text{H}_2\text{O}$  derived from perturbation-theory energy levels. *Theor. Chem. Acc.* **1988**, *74*, 493–511.
- (59) Isaacson, A. D.; Hung, S.-C. Use of second-order perturbation theory for the vibrational energy levels and partition functions at a saddle point. *J. Chem. Phys.* **1994**, *101*, 3928–3935.
- (60) Kuhler, K. M.; Truhlar, D. G.; Isaacson, A. D. General method for removing resonance singularities in quantum mechanical perturbation theory. *J. Chem. Phys.* **1996**, *104*, 4664–4670.
- (61) Isaacson, A. D. Removing resonance effects from quantum mechanical vibrational partition functions obtained from perturbation theory. *J. Chem. Phys.* **1998**, *108*, 9978–9986.
- (62) Daněček, P.; Bouř, P. Comparison of the numerical stability of methods for anharmonic calculations of vibrational molecular energies. *J. Comput. Chem.* **2007**, *28*, 1617–1624.
- (63) Respondek, I.; Benoit, D. M. Fast degenerate correlation-corrected vibrational self-consistent field calculations of the vibrational spectrum of 4-mercaptopyridine. *J. Chem. Phys.* **2009**, *131*, 054109.
- (64) Schuurman, M. S.; Allen, W. D.; von Ragué Schleyer, P.; Schaefer, H. F. III. The highly anharmonic  $\text{BH}_3$  potential energy surface characterized in the ab initio limit. *J. Chem. Phys.* **2005**, *122*, 104302.
- (65) Tomasi, J.; Mennucci, B.; Cammi, R. Quantum Mechanical Continuum Solvation Models. *Chem. Rev.* **2005**, *105*, 2999.
- (66) Cossi, M.; Scalmani, G.; Rega, N.; Barone, V. Energies, Gradients, and harmonic frequencies for molecules in solution by the C-PCM solvation model. *J. Comput. Chem.* **2003**, *24*, 669.
- (67) Scalmani, G.; Barone, V.; Kudin, K.; Pomelli, C.; Scuseria, G.; Frisch, M. Achieving linear-scaling computational cost for the polarizable continuum model of solvation. *Theor. Chem. Acc.* **2004**, *111*, 90.
- (68) Cappelli, C.; Lipparini, F.; Bloino, J.; Barone, V. Towards an accurate description of anharmonic infrared spectra in solution within the polarizable continuum model: Reaction field, cavity field and nonequilibrium effects. *J. Chem. Phys.* **2011**, *135*, 104505. Erratum: *ibidem* **2011**, *135*, 149901.
- (69) Miller, W. H.; Hernandez, R.; Handy, N. C.; Jayatilaka, D.; Willets, A. Ab initio calculation of anharmonic constants for a transition state, with application to semiclassical transition state tunneling probabilities. *Chem. Phys. Lett.* **1990**, *172*, 62–68.
- (70) Darling, B. T.; Dennison, D. M. The Water Vapor Molecule. *Phys. Rev.* **1940**, *57*, 128–139.
- (71) Fermi, E. Über den Ramaneffekt des Kohlendioxyds. *Z. Phys. A: Hadrons Nucl.* **1931**, *71*, 250–259.
- (72) Becke, A. D. Density-functional thermochemistry. III. The role of exact exchange. *J. Chem. Phys.* **1993**, *98*, 5648.
- (73) Double and triple- $\zeta$  basis sets of N07 family are available for download. Visit <http://idea.sns.it> (accessed November 10, 2011).
- (74) Barone, V.; Cimino, P.; Stendardo, E. Development and Validation of the B3LYP/N07D Computational Model for Structural Parameter and Magnetic Tensors of Large Free Radicals. *J. Chem. Theory Comput.* **2008**, *4*, 751.



- (75) Barone, V.; Cimino, P. Accurate and feasible computations of structural and magnetic properties of large free radicals: The PBE0/N07D model. *Chem. Phys. Lett.* **2008**, *454*, 139–143.
- (76) Barone, V.; Cimino, P. Validation of the B3LYP/N07D and PBE0/N07D Computational Models for the Calculation of Electronic g-Tensors. *J. Chem. Theory Comput.* **2009**, *5*, 192–199.
- (77) Barone, V.; Biczysko, M.; Bloino, J.; Borkowska-Panek, M.; Carnimeo, I.; Panek, P. Toward anharmonic computations of vibrational spectra for large molecular systems. *Int. J. Quantum Chem.* **2011**, DOI: 10.1002/qua.23224.
- (78) Carnimeo, I.; Biczysko, M.; Bloino, J.; Barone, V. Reliable structural, thermodynamic, and spectroscopic properties of organic molecules adsorbed on silicon surfaces from computational modeling: the case of glycine@Si(100). *Phys. Chem. Chem. Phys.* **2011**, *13*, 16713–16727.
- (79) Grimme, S. Semiempirical hybrid density functional with perturbative second-order correlation. *J. Chem. Phys.* **2006**, *124*, 034108.
- (80) Dunning, T. H. Gaussian basis sets for use in correlated molecular calculations. I. The atoms boron through neon and hydrogen. *J. Chem. Phys.* **1989**, *90*, 1007.
- (81) Kendall, R. A.; Dunning, T. H.; Harrison, R. J. Electron affinities of the first-row atoms revisited. Systematic basis sets and wave functions. *J. Chem. Phys.* **1992**, *96*, 6796.
- (82) Barone, V.; Festa, G.; Grandi, A.; Rega, N.; Sanna, N. Accurate vibrational spectra of large molecules by density functional computations beyond the harmonic approximation: the case of uracil and 2-thiouracil. *Chem. Phys. Lett.* **2004**, *388*, 279–283.
- (83) Puzzarini, C.; Biczysko, M.; Barone, V. Accurate anharmonic vibrational frequencies for uracil: the performance of composite schemes and hybrid CC/DFT model. *J. Chem. Theory Comput.* **2011**, *7*, 3702–3710.
- (84) Frisch, M. J.; Trucks, G. W.; Schlegel, H. B.; Scuseria, G. E.; Robb, M. A.; Cheeseman, J. R.; Scalmani, G.; Barone, V.; Mennucci, B.; Petersson, G. A.; Nakatsuji, H.; Caricato, M.; Li, X.; Hratchian, H. P.; Izmaylov, A. F.; Bloino, J.; Zheng, G.; Sonnenberg, J. L.; Liang, W.; Hada, M.; Ehara, M.; Toyota, K.; Fukuda, R.; Hasegawa, J.; Ishida, M.; Nakajima, T.; Honda, Y.; Kitao, O.; Nakai, H.; Vreven, T.; Montgomery, J. A., Jr.; Peralta, J. E.; Ogliaro, F.; Bearpark, M.; Heyd, J. J.; Brothers, E.; Kudin, K. N.; Staroverov, V. N.; Keith, T.; Kobayashi, R.; Normand, J.; Raghavachari, K.; Rendell, A.; Burant, J. C.; Iyengar, S. S.; Tomasi, J.; Cossi, M.; Rega, N.; Millam, J. M.; Klene, M.; Knox, J. E.; Cross, J. B.; Bakken, V.; Adamo, C.; Jaramillo, J.; Gomperts, R.; Stratmann, R. E.; Yazyev, O.; Austin, A. J.; Cammi, R.; Pomelli, C.; Ochterski, J. W.; Martin, R. L.; Morokuma, K.; Zakrzewski, V. G.; Voth, G. A.; Salvador, P.; Dannenberg, J. J.; Dapprich, S.; Parandekar, P. V.; Mayhall, N. J.; Daniels, A. D.; Farkas, O.; Foresman, J. B.; Ortiz, J. V.; Cioslowski, J.; Fox, D. J. *Gaussian Development Version*, revision H.13. Gaussian, Inc.: Wallingford, CT, 2010.
- (85) Irikura, K. K. Experimental Vibrational Zero-Point Energies: Diatomic Molecules. *J. Phys. Chem. Ref. Data* **2007**, *36*, 389–397.
- (86) Kolmann, S. J.; Jordan, M. J. T. Method and basis set dependence of anharmonic ground state nuclear wave functions and zero-point energies: Application to SSSH. *J. Chem. Phys.* **2010**, *132*, 054105.
- (87) Zuniga, J.; Picon, J. A. G.; Bastida, A.; Requena, A. On the use of optimal internal vibrational coordinates for symmetrical bent triatomic molecules. *J. Chem. Phys.* **2005**, *122*, 224319.
- (88) Puzzarini, C. Ab initio characterization of  $\text{XH}_3$  ( $X = \text{N}, \text{P}$ ). Part II. Electric, magnetic and spectroscopic properties of ammonia and phosphine. *Theor. Chem. Acc.* **2008**, *121*, 1–10.
- (89) Rajamaki, T.; Miani, A.; Halonen, L. Vibrational energy levels for symmetric and asymmetric isotopomers of ammonia with an exact kinetic energy operator and new potential energy surfaces. *J. Chem. Phys.* **2003**, *118*, 6358–6369.
- (90) Bokareva, O.; Bataev, V.; Godunov, I. A quantum-chemical study of the structure and conformational dynamics of the acrolein molecule in the ground electronic state. *Russ. J. Phys. Chem. A* **2009**, *83*, 81–90.
- (91) Denis, P. On the enthalpy of formation of thiophene. *Theor. Chem. Acc.* **2010**, *127*, 621–626.
- (92) Denis, P. Coupled cluster, B2PLYP and M06–2X investigation of the thermochemistry of five-membered nitrogen containing heterocycles, furan, and thiophene. *Theor. Chem. Acc.* **2011**, *129*, 219–227.
- (93) Wang, Y.; Braams, B. J.; Bowman, J. M.; Carter, S.; Tew, D. P. Full-dimensional quantum calculations of ground-state tunneling splitting of malonaldehyde using an accurate ab initio potential energy surface. *J. Chem. Phys.* **2008**, *128*, 224314.
- (94) Csonka, G. I.; Ruzsinszky, A.; Perdew, J. P. Estimation, Computation, and Experimental Correction of Molecular Zero-Point Vibrational Energies. *J. Phys. Chem. A* **2005**, *109*, 6779–6789.
- (95) McClurg, R. B.; Flagan, R. C.; Goddard, W. A. III. The hindered rotor density-of-states interpolation function. *J. Chem. Phys.* **1997**, *106*, 6675–6680.
- (96) Ayala, P. Y.; Schlegel, H. B. Identification and treatment of internal rotation in normal mode vibrational analysis. *J. Phys. Chem.* **1998**, *108*, 2314–2325.
- (97) McClurg, R. B. Comment on: The hindered rotor density-of-states interpolation function [J. Chem. Phys. 106, 6675 (1997)] and The hindered rotor density- of-states [J. Chem. Phys. 108, 2314 (1998)]. *J. Chem. Phys.* **1999**, *111*, 7163–7164.
- (98) Hoy, A.; Mills, I.; Strey, G. Anharmonic force constant calculations. *Mol. Phys.* **1972**, *24*, 1265–1290.
- (99) Pitzer, K. S.; Gwinn, W. D. Energy Levels and Thermodynamic Functions for Molecules with Internal Rotation I. Rigid Frame with Attached Tops. *J. Chem. Phys.* **1942**, *10*, 428–440.
- (100) Li, J. C. M.; Pitzer, K. S. Energy Levels and Thermodynamic Functions for Molecules with Internal Rotation. IV. Extended Tables for Molecules with Small Moments of Inertia. *J. Phys. Chem.* **1956**, *60*, 466–474.
- (101) Truhlar, D. G. A simple approximation for the vibrational partition function of a hindered internal rotation. *J. Comput. Chem.* **1991**, *12*, 266–270.
- (102) Chuang, Y.-Y.; Truhlar, D. G. Statistical thermodynamics of bond torsional modes. *J. Chem. Phys.* **2000**, *112*, 1221–1228.
- (103) Block, D. A.; Armstrong, D. A.; Rauk, A. Gas Phase Free Energies of Formation and Free Energies of Solution of “C-Centered Free Radicals from Alcohols: A Quantum Mechanical-Monte Carlo Study. *J. Phys. Chem. A* **1999**, *103*, 3562–3568.
- (104) Guthrie, J. P. Use of DFT Methods for the Calculation of the Entropy of Gas Phase Organic Molecules: An Examination of the Quality of Results from a Simple Approach. *J. Phys. Chem. A* **2001**, *105*, 8495–8499.
- (105) Suarez, E.; Diaz, N.; Suarez, D. Entropy Calculations of Single Molecules by Combining the Rigid-Rotor and Harmonic-Oscillator Approximations with Conformational Entropy Estimations from Molecular Dynamics Simulations. *J. Chem. Theory Comput.* **2011**, *7*, 2638–2653.
- (106) Stepanian, S. G.; Reva, I. D.; Radchenko, E. D.; Rosado, M. T. S.; Duarte, M. L. T. S.; Fausto, R.; Adamowicz, L. Matrix-Isolation Infrared and Theoretical Studies of the Glycine Conformers. *J. Phys. Chem. A* **1998**, *102*, 1041–1054.
- (107) Graindourze, M.; Smets, J.; Zeegers-Huyskens, T.; Maes, G. Fourier transform-infrared spectroscopic study of uracil derivatives and their hydrogen bonded complexes with proton donors: Part I. Monomer infrared absorptions of uracil and some methylated uracils in argon matrices. *J. Mol. Struct.* **1990**, *222*, 345–364.
- (108) Szczesniak, M.; Nowak, M. J.; Rostkowska, H.; Szczepaniak, K.; Person, W. B.; Shugar, D. Matrix isolation studies of nucleic acid constituents. 1. Infrared spectra of uracil monomers. *J. Am. Chem. Soc.* **1983**, *105*, 5969–5976.
- (109) Chin, S.; Scott, I.; Szczepaniak, K.; Person, W. B. Matrix isolation studies of nucleic acid constituents. 2. Quantitative ab initio prediction of the infrared spectrum of in-plane modes of uracil. *J. Am. Chem. Soc.* **1984**, *106*, 3415–3422.

- (110) Breda, S.; Reva, I. D.; Lapinski, L.; Nowak, M. J.; Fausto, R. Infrared spectra of pyrazine, pyrimidine and pyridazine in solid argon. *J. Mol. Struct.* **2006**, *786*, 193–206.
- (111) Bloino, J.; Barone, V. A VPT2 route to vibrational spectroscopy: general formulation and application to spectroscopic properties. *J. Chem. Phys.* **2012**, submitted.
- (112) Duncan, J.; Law, M. A study of vibrational anharmonicity, fermi resonance interactions, and local mode behavior in CH<sub>3</sub>Cl. *J. Mol. Spectrosc.* **1990**, *140*, 13–30.
- (113) Schryber, J. H.; Polyansky, O. L.; Jensen, P.; Tennyson, J. On the Spectroscopically Determined Potential Energy Surfaces for the Electronic Ground States of NO<sub>2</sub> and H<sub>2</sub>O. *J. Mol. Spectrosc.* **1997**, *185*, 234–243.
- (114) Hamada, Y.; Nishimura, Y.; Tsuboi, M. Infrared spectrum of trans-acrolein. *Chem. Phys.* **1985**, *100*, 365–375.
- (115) Huisken, F.; Werhahn, O.; Ivanov, A.; Krasnokutski, S. The O-H stretching vibrations of glycine trapped in rare gas matrices and helium clusters. *J. Chem. Phys.* **1999**, *111*, 2978.
- (116) Klots, T.; Chirico, R.; Steele, W. Complete vapor phase assignment for the fundamental vibrations of furan, pyrrole and thiophene. *Spectrochim. Acta A* **1994**, *50*, 765–795.
- (117) Mellouki, A.; Lievin, J.; Herman, M. The vibrational spectrum of pyrrole (C<sub>4</sub>H<sub>5</sub>N) and furan (C<sub>4</sub>H<sub>4</sub>O) in the gas phase. *Chem. Phys.* **2001**, *271*, 239–266.
- (118) Chiavassa, T.; Roubin, P.; Pizzala, L.; Verlaque, P.; Allouche, A.; Marinelli, F. Experimental and theoretical studies of malonaldehyde: vibrational analysis of a strongly intramolecularly hydrogen bonded compound. *J. Phys. Chem.* **1992**, *96*, 10659–10665.
- (119) Turner, P.; Baughcum, S. L.; Coy, S. L.; Smith, Z. Microwave spectroscopic study of malonaldehyde. 4. Vibration-rotation interaction in parent species. *J. Am. Chem. Soc.* **1984**, *106*, 2265–2267.
- (120) Barone, V.; Adamo, C. Proton transfer in the ground and lowest excited states of malonaldehyde: A comparative density functional and post-Hartree-Fock study. *J. Chem. Phys.* **1996**, *105*, 11007–11019.
- (121) Klots, T. Raman vapor spectrum and vibrational assignment for pyridine. *Spectrochim. Acta A* **1998**, *54*, 1481–1498.
- (122) Chase, M. NIST-JANAF Thermochemical Tables, 4th Edition. *J. Phys. Chem. Ref. Data* **1998**, *9*, 1–1951.
- (123) Chao, J.; Hall, K. R.; Marsh, K. N.; Wilhoit, R. C. Thermodynamic Properties of Key Organic Oxygen Compounds in the Carbon Range C1 to C4. Part 2. Ideal Gas Properties. *J. Phys. Chem. Ref. Data* **1986**, *15*, 1369–1436.
- (124) Dean, J. *Lange's Handbook of Chemistry*; McGraw-Hill: New York, 1985.
- (125) Dorofeeva, O. V.; Novikov, V. P.; Neumann, D. B. NIST-JANAF Thermochemical Tables. I. Ten Organic Molecules Related to Atmospheric Chemistry. *J. Phys. Chem. Ref. Data* **2001**, *30*, 475–513.
- (126) Tennyson, J.; Zobov, N. F.; Williamson, R.; Polyansky, O. L.; Bernath, P. F. Experimental Energy Levels of the Water Molecule. *J. Phys. Chem. Ref. Data* **2001**, *30*, 735–831.
- (127) Sappey, A. D.; Crosley, D. R. Laser-induced fluorescence in the B-X system of the HCO radical. *J. Chem. Phys.* **1990**, *93*, 7601–7608.
- (128) McKellar, A.; Vervloet, M.; Burkholder, J.; Howard, C. A combined analysis of the  $\nu_1$ ,  $\nu_3$ , and  $2\nu_2$  vibrational states of the NH<sub>2</sub> radical using Fourier transform absorption and emission data. *J. Mol. Struct.* **1990**, *142*, 319–335.
- (129) Burkholder, J.; Howard, C.; McKellar, A. Fourier transform infrared spectrum of the  $\nu_2$  band of the NH<sub>2</sub> radical. *J. Mol. Struct.* **1988**, *127*, 415.
- (130) Spirko, V.; Kraemer, W. Anharmonic potential function and effective geometries for the NH<sub>3</sub> molecule. *J. Mol. Spectrosc.* **1989**, *133*, 331–344.
- (131) Kleiner, I.; Brown, L.; Tarrago, G.; Kou, Q.-L.; Picque, N.; Guelachvili, G.; Dana, V.; Mandin, J.-Y. Positions and Intensities in the  $2\nu_4/\nu_1/\nu_3$  Vibrational System of <sup>14</sup>NH<sub>3</sub> Near 3  $\mu$ m. *J. Mol. Spectrosc.* **1999**, *193*, 46–71.
- (132) Cottaz, C.; Kleiner, I.; Tarrago, G.; Brown, L.; Margolis, J.; Poynter, R.; Pickett, H.; Fouchet, T.; Drossart, P.; Lellouch, E. Line Positions and Intensities in the  $2\nu_2/\nu_4$  Vibrational System of <sup>14</sup>NH<sub>3</sub> Near 5–7  $\mu$ m. *J. Mol. Spectrosc.* **2000**, *203*, 285–309.
- (133) Feller, D.; Peterson, K. A. High level coupled cluster determination of the structure, frequencies, and heat of formation of water. *J. Chem. Phys.* **2009**, *131*, 154306.
- (134) Marenich, A. V.; Boggs, J. E. Coupled Cluster CCSD(T) Calculations of Equilibrium Geometries, Anharmonic Force Fields, and Thermodynamic Properties of the Formyl (HCO) and Isoformyl (COH) Radical Species. *J. Phys. Chem. A* **2003**, *107*, 2343–2350.
- (135) Biczysko, M.; Bloino, J.; Carnimeo, I.; Panek, P.; Barone, V. Fully ab initio IR spectra for complex molecular systems from perturbative vibrational approaches: Glycine as a test case. *J. Mol. Struct.* **2012**, *1009*, 74–82.